AD_____
(Leave blank)

Award Number:
W81XWH-09-1-0187

TITLE:
Role of Nonreceptor Protein Kinase Ack1 in Prostate Cancer

PRINCIPAL INVESTIGATOR:
Charlene Rivera

CONTRACTING ORGANIZATION:
University of North Carolina at Chapel Hill
Chapel Hill, NC 27599-0001

REPORT DATE:
May 2010

TYPE OF REPORT:
Annual Summary

PREPARED FOR: U.S. Army Medical Research and Materiel Command
Fort Detrick, Maryland 21702-5012

DISTRIBUTION STATEMENT: (Check one)

X Approved for public release; distribution unlimited

☐ Distribution limited to U.S. Government agencies only; report contains proprietary information

The views, opinions and/or findings contained in this report are those of the author(s) and should not be construed as an official Department of the Army position, policy or decision unless so designated by other documentation

REPORT DOCUMENTATION PAGE

Form Approved
OMB No. 0704-0188

1. REPORT DATE *(DD-MM-YYYY)*	2. REPORT TYPE	3. DATES COVERED *(From - To)*
01-05-2010	Annual Summary	1 May 2009 - 30 Apr 2010

4. TITLE AND SUBTITLE
Role of Nonreceptor Tyrosine Kinase Ack1 in Prostate Cancer

5a. CONTRACT NUMBER
W81XWH-09-1-0187

5b. GRANT NUMBER

5c. PROGRAM ELEMENT NUMBER

6. AUTHOR(S)
Charlene Rivera

Email: crivera@med.unc.edu

5d. PROJECT NUMBER

5e. TASK NUMBER

5f. WORK UNIT NUMBER

7. PERFORMING ORGANIZATION NAME(S) AND ADDRESS(ES)
University of North Carolina at Chapel Hill

104 Airport Dr, CB 1350
Chapel Hill, NC 27599-0001

8. PERFORMING ORGANIZATION REPORT NUMBER

9. SPONSORING / MONITORING AGENCY NAME(S) AND ADDRESS(ES)
U.S. Army Medical Research and Materiel Command
Fort Detrick, Maryland 21702-5012

10. SPONSOR/MONITOR'S ACRONYM(S)

11. SPONSOR/MONITOR'S REPORT NUMBER(S)

12. DISTRIBUTION / AVAILABILITY STATEMENT
Approved for public release; distribution unlimited

13. SUPPLEMENTARY NOTES

14. ABSTRACT Recent studies from our laboratory have shown that constitutively active Ack1 directly binds and tyrosine phosphorylates the androgen receptor (AR), resulting in ligand-independent AR activity. Moreover, Ack1 transforms LNCaP cells into androgen-independent and highly invasive tumors in nude mice. However, the role of Ack-1 in prostate cancer initiation and progression within the context of a complex organ remains poorly understood. To address this question, we generated transgenic mice expressing a myc-tagged constitutively activate Ack1 transgene in the prostate epithelium, driven by a modified rat *probasin* promoter. Furthermore, *Pb-Ack1* mice were crossed to genetically engineered mice ($PTEN^{+/-}$ and $TgAP\text{-}T_{121}$) that develop high-grade prostate intraepithelial neoplasias (PIN) or adenocarcinoma**.** *Pb-Ack1* prostates presented focal hyperplasia and nuclear atypia as early as 16 weeks of age. These prostatic lesions progressed to mPIN and microinvasive carcinoma as detected in prostates from 49 weeks old *Pb-Ack1* mice. Crossing of *Pb-Ack1* mice to $TgAPT_{121}$ mice resulted in accelerated onset of progressive CaP which was detected as early as 24 weeks of age. Furthermore, the apoptotic index was reduced by 50% in bi-transgenic prostates when compared to single $TgAPT_{121}$ prostates. An increase in serine-phospho-p65 was also observed in the bi-transgenic when compared to the $TgAPT_{121}$ prostates. *Pb-Ack1;*$Pten^{+/-}$ compound mice presented mPIN lesions as early as 16 weeks of age. Phospho-serine Akt was detected exclusively in these mPIN lesions, suggesting PTEN loss of heterozygosity. In summary, these data present evidence that Ack-1's oncogenic activity can promote the initiation and progression of prostate cancer *in vivo*.

15. SUBJECT TERMS
Prostate cancer, transgenic mice, mouse model

16. SECURITY CLASSIFICATION OF:			17. LIMITATION OF ABSTRACT	18. NUMBER OF PAGES	19a. NAME OF RESPONSIBLE PERSON
a. REPORT	b. ABSTRACT	c. THIS PAGE			USAMRMC
U	U	U	UU	38	19b. TELEPHONE NUMBER *(include area code)*

Standard Form 298 (Rev. 8-98)
Prescribed by ANSI Std. Z39.18

Table of Contents

Page

Introduction

In its initial stages prostate cancer depends on androgen signaling, with androgen ablation therapy inducing tumor regression. The disease becomes extremely difficult to treat when it progresses to a hormone refractory state (androgen-independent prostate cancer or AICaP), therefore making it the second leading cause of cancer related death among men in the United States. Dissecting the molecular mechanisms underlying prostate cancer initiation and progression to AICaP will allow us to develop more efficient therapeutics and reduce the mortality rates of patients. Recent studies from our laboratory have shown that a constitutively active form of the intracellular tyrosine kinase Ack1 (activated cdc42-associated tyrosine kinase) directly binds and tyrosine phosphorylates the androgen receptor (AR), resulting in ligand-independent AR activity [1-2]. Constitutive activation was achieved by introducing a mutation that relieves kinase auto-inhibition (L487F) and by COOH-terminal truncation (amino acids 788-1,036) [3]. Moreover, caAck1 transforms poorly tumorigenic LNCaP cells into androgen-independent and highly invasive tumors in nude mice [1]. However, the role of Ack-1 in prostate cancer initiation and progression within the context of a complex organ remains poorly understood. To address this question, transgenic mice were generated expressing a myc-tagged truncated caAck1 transgene in the prostate epithelium, driven by a modified rat *probasin* promoter which contains two copies of the androgen response region (ARR2PB promoter). Characterization of these transgenic (*Pb-Ack1*) mice would allow us to understand the mechanisms through which this novel tyrosine kinase maybe drive the progression of prostate cancer *in vivo* as well as to further understand its potential role in AICaP. Furthermore, *Pb-Ack1* mice were crossed to genetically engineered mice ($Pten^{+/-}$ and $TgAP\text{-}T_{121}$) that develop high-

grade prostate intraepithelial neoplasias (PIN) or adenocarcinoma at known rates in order to understand how Ack1 activity, in combination with other lesions, will result in invasive and metastatic adenocarcinomas, thus reflecting the pathophysiology of human AICaP**.** *Pten*$^{+/-}$ and *TgAP-T*$_{121}$ were chosen for the relevance of *PTEN* and *Rb* mutations in human prostate cancer as well as for the defined kinetics of cancer initiation and progression in these genetically engineered mice model of prostate cancer [4-5].

Body

The Statement of Work of the present study aimed at: 1) determining if prostate-specific expression of caAck1 resulted in the formation of metastatic adenocarcinomas through increased growth and survival of prostate epithelial cells, 2) determining if prostate-specific expression of caAck1 resulted in androgen-independence growth and survival, 3) examining if the expression of *caAck1* in established mouse models of prostate cancer resulted in accelerated tumor formation and metastasis and 4) determining if prostate-specific expression of caAck1 resulted in androgen- independence growth and survival when crossed to $Pten^{+/-}$ and $TgAP\text{-}T_{121}$ mice. In order to address these tasks, transgenic mice were generated by expressing a myc-tagged constitutively activated Ack1 transgene in the prostate epithelium, driven by a modified rat *probasin* promoter which contains two copies of the androgen response region (ARR2PB promoter). Furthermore, *Pb-Ack1* mice were crossed to genetically engineered mice $Pten^{+/-}$and $TgAP\text{-}T_{121}$. These mice constructs were chosen for the relevance of *PTEN* and *Rb* mutations in human prostate cancer as well as for the defined kinetics of cancer initiation and progression in these genetically engineered mice model of prostate cancer [4-5].

Task 1

For task 1, prostates from *Pb-Ack1* mice and non-transgenic littermates were collected at multiple time points (12, 16, 24, 36, 48 and 72 weeks of age). Histopathological analysis of hematoxylin and eosin (H&E) stained paraffin sections showed that *Pb-Ack1* prostates presented focal hyperplasia accompanied by nuclear atypia as early as 16 weeks of age. These prostatic lesions appeared to progress as evidenced by the presence of murine prostatic intraepithelial neoplasia (mPIN) and microinvasive carcinoma by 49 weeks of age (Appendix Fig. 1). This

later phenotype was detected in one mouse and was determined by the extension of small acini of cytologically atypical cells into the fibromuscular layer (Appendix Fig. 1). mPIN lesions were multifocal in this specimen and displayed a cribiform pattern which resulted from further stratification of the epithelial layer and were accompanied by further cellular atypia (spindle-like shaped cells) and nuclear atypia (nuclear elongation and hyperchromatia) as well as hypercellularity of the stromal layer (Appendix Fig. 1). Desmoplasia (a disruption of the fibromuscular layer often seen in microinvasive adenocarcinoma) was detected by smooth muscle-actin immunohistochemistry on paraffin sections (Appendix Fig. 2). Double immunofluorescence detection of Ki67 (a proliferation marker) and cytokeratin 8 (a luminal epithelial marker) on paraffin sections showed increased cell proliferation in the *Pb-Ack1* prostate epithelium when compared to WT (Appendix Fig. 3). The histopathological phenotype of *Pb-Ack1* was published in PLoS ONE (see Appendix).

Task 3

For task 3, *Pb-Ack1* mice were crossed to *TgAPT*$_{121}$ mice. These transgenic mice were generated in the laboratory of our collaborator Dr. Terry Van Dyke and are a mouse model of prostate cancer in which T121 (a portion of the large T antigen) exclusively targets and inactivates all members of the pRb family [4]. Transgenic expression of T121 to prostate epithelial cells (*TgAP-T*$_{121}$ mice) results in rapid formation of neoplasias that are derived from luminal epithelial cells. mPIN in *TgAP-T*$_{121}$ mice develop by 12 weeks of age and progress to micro-invasive adenocarcinomas by 30 weeks of age. Metastasis has not been reported in these mice [4]. Expression of caAck1 in the *TgAP-T*$_{121}$ background resulted in accelerated onset of the adeno-progressive phenotype which was detected as early as 24 weeks of age and determined by

H&E staining of paraffin slides (Appendix Fig. 4). Although the adeno-progressive phenotype was also observed some single *TgAP-T_{121}* prostates within our cohort, it was not as penetrant (30%) as in the *PbAck1;TgAP-T_{121}* bi-transgenic (86%). Furthermore, the apoptotic index was reduced in *PbAck1;TgAP-T_{121}* bi-transgenic prostates when compared to single *TgAPT$_{121}$* prostates at 16 and 24 weeks of age (Appendix Fig. 5). Apoptotic cells were detected *in situ* by TUNEL (Terminal dUTP Nick End Labeling) analysis on paraffin sections from 3 WT, *PbAck1*, *TgAP-T_{121}*, and *Pb-Ack1;TgAP-T_{121}* prostates at 16 and 24 weeks of age. Apoptotic indexes were calculated by counting TUNEL-positive cells (brown, arrows) as a percentage of total cells (hematoxylin). Data were analyzed by Wilcoxon test ($P<0.05$ is considered statistically significant). In addition, an increase in NFκB activation was observed in the bi-transgenic prostates as early as 16 weeks of age ($p=0.025$) when compared to the *TgAPT$_{121}$* prostates (Appendix Fig. 6). NFκB activation was detected *in situ* by serine-phospho-p65 immunohistochemistry on paraffin slides from at least 3 WT, *PbAck1*, *TgAP-T_{121}*, and *Pb-Ack1;TgAP-T_{121}* prostates at 16 and 24 weeks of age and analyzed as described above.

The microarray analysis proposed in this task is currently underway. RNA was isolated from anterior prostates of WT, *PbAck1*, *TgAP-T_{121}* and *PbAck1;TgAP-T_{121}* mice. RNA from three mice per genotype at 16 and 24 weeks of age were submitted for microarray analysis to the UNC Lineberger Comprehensive Cancer Center Genomics and Bioinformatics Core. A universal mouse reference comprised of total mouse embryonic RNA Universal mouse reference RNA was used as control. Data will be analyzed using the Signifance Analysis of Microarrays (SAM) freeware.

Pb-Ack1 mice were also crossed to *Pten$^{+/-}$* mice as proposed in task 3. Formation of mPIN from secretory prostate epithelial cells, progression to prostate cancer (CaP), and

formation of metastasis has been observed in mice with prostate-specific *PTEN* disruption [2]. Heterozygotic loss of *PTEN* causes prostate cancer at known rates, with most *Pten*$^{+/-}$ mice developing LGPIN at around 6 months of age, and homozygote conditional ablation of *PTEN* in the mouse prostate resulting in mPIN at 6 weeks of age, CaP at 9 weeks of age, and metastasis at 12 weeks of age [2, 5]. This mouse model is highly relevant to the human disease given that the *PTEN* gene is often subject to loss of heterozygosity (LOH) in human prostate cancer [6]. Our preliminary data showed that *Pb-Ack1;Pten*$^{+/-}$ mice present mPIN lesions as early as 16 weeks of age as determined by H&E staining of paraffin sections (Fig. 7). The onset of the mPIN phenotype is accelerated in *Pb-Ack1;Pten*$^{+/-}$ prostates by approximately 32 weeks when compared to *Pb-Ack1* and *Pten*$^{+/-}$ prostates. These mPIN lesions present abnormal tufting glandular patterns with multiple cellular atypia including nuclear enlargement, inversion of nuclear to cytoplasmic ratio and hyperchromatism. The detection of Ki67 showed that these mPIN lesions were highly comprised of proliferating cells (Appendix Fig. 8). Ki67 was detected *in situ* by Ki67 immunohistochemistry on paraffin slides. Furthermore, abnormal cells within these mPIN lesions were positive for phosphorylated (activated) Akt, suggesting PTEN LOH (Appendix Fig. 9). Activated Akt was detected *in situ* by serine-phospho-Akt immunohistochemistry on paraffin slides. PTEN LOH is further suggested by the loss of PTEN staining in phospho-Akt positive cells, detected by immunohistochemistry of sequential slides from *Pb-Ack1;Pten*$^{+/-}$ prostates (Appendix Fig. 10). Despite the acceleration of the mPIN phenotype in the *Pb-Ack1;Pten*$^{+/-}$ as compared to the single *Pb-Ack1* or *Pten*$^{+/-}$, progression to adenocarcinoma was not observed in these compound mice by 48 weeks of age as determined by H&E staining of paraffin slides (Appendix Fig. 7). To date, at least 3 *Pb-Ack1* and 3 *Pb-Ack1;Pten*$^{+/-}$ mice have been characterized.

Task 2, 4

I expect to conduct the androgen-ablation experiments described in Aim 1, Part 3 and Aim 2, Part 5 later in 2010. This will be done on WT, *Pb-Ack1*, *Pten*$^{+/-}$ and *Pb-Ack1;Pten*$^{+/-}$ animals and I will follow the methodology previously described in the fellowship.

Key Research Accomplishments

- Provided evidence showing that expression of truncated caAck1 is sufficient to cause to a prostatic phenotype when expressed in the prostate epithelium *in vivo*.
- Provided evidence showing that truncated caAck1 can lead to accelerated onset of prostatic phenotype when co-expressed in murine models of prostate cancer *TgAP-*T_{121} and *Pten*$^{+/-}$.
- Provided evidence showing that expression of truncated caAck1 signals a cell survival pathway *in vivo* which rescues the apoptotic phenotype when co-expressed in *TgAP-*T_{121} mice.
- Provided evidence showing that expression of truncated caAck1 leads to increased activation of NFκB when co-expressed in *TgAP-*T_{121} mice.

Reportable Outcomes

- Mahajan, K., Coppola, D., Challa, S., Fang, B., Chen, Y.A., Zhu, W., Lopez, A.S., Koomen, J., Engelman, R.W., **Rivera, C.**, Muraoka-Cook, R.S., Cheng, J.Q., Schönbrunn, E., Sebti, S.M., Earp, H.S., and Mahajan, N.P. Ack1 Mediated AKT/PKB Tyrosine 176 Phosphorylation Regulates Its Activity. PLoS ONE 2010;5(3):e9646

Conclusions

I assessed the effect of Ack1 activity *in vivo* by directing cell-specific expression of caAck1 to the murine prostate epithelium. The data present evidence for caAck-1 expression to be sufficient to deregulate proper cell cycle of luminal epithelial cells. This deregulation led to a hyperplastic phenotype that progressed to mPIN and in one case to adenocarcinoma. Furthermore, caAck1 activity was shown to accelerate the onset of the prostatic phenotype when crossed to both *Pten*$^{+/-}$ and *TgAP-T*$_{121}$ mice, thus supporting our hypothesis that Ack1 activity in the murine prostate epithelium, in combination with precursor lesions, would result in a more aggressive phenotype.

The *TgAP-T*$_{121}$ mice were generated by our collaborator Dr. Terry Van Dyke. I initially focused on this transgenic construct given that complete inactivation of pRb function was shown to initiate and progress prostate tumorigenesis at well characterized rates. When crossed to the *TgAP-T*$_{121}$ mice, caAck1 was able to accelerate the onset of the prostate adeno-progressive phenotype from 30 weeks in the single *TgAP-T*$_{121}$ transgenic to 24 weeks in the *PbAk1*; *TgAP-T*$_{121}$ bi-transgenic construct. This acceleration correlated with caAck1's ability to induce a pro-survival signal in these bi-transgenic prostates, which may explain the reduction in apoptosis observed in the *PbAk1*; *TgAP-T*$_{121}$ bi-transgenic prostates. A pro-survival role for Ack1 has already been reported in NIH 3T3 cells [7]. Ack1 was shown to be required for the survival of v-Ras-transformed cells, although the cell survival signal remains to be elucidated [7]. Here I showed that the reduction of apoptosis in *PbAk1*; *TgAP-T*$_{121}$ bi-transgenic directly correlated with an increased in activation and nuclear localization of NFκB, thus providing a molecular mechanism through which Ack1 may be elucidating its cell survival signal.

In addition, *PbAk1* mice were also crossed to *Pten*$^{+/-}$ mice in order to assess the effects of Ack1 activity along with reduction of Pten gene dosage. This construct was chosen given the

high frequency of Pten mutation or reduced gene expression observed in human prostate cancer [6]. It has been previously reported that *Pten*$^{+/-}$ male mice develop prostate hyperplasia or mPIN at around 9-14 months of age [2, 5]. Here, I observed that the compound *PbAk1*; *Pten*$^{+/-}$ male mice develop mPIN as early as 16 weeks, whereas this prostatic phenotype is not seen until approximately 32 weeks in the *PbAk1* or *Pten*$^{+/-}$ male mice in the same experimental cohort. Furthermore, the activation of Akt within these mPIN lesions suggests Ack1 activity may be providing the selective pressure needed for inactivation of Pten through LOH. Despite the accelerated mPIN phenotype in *PbAk1*; *Pten*$^{+/-}$ male mice, the phenotype fails to progress to adenocarcinoma or metastasis. Addressing the experiments proposed in tasks 2 and 4 will allow me to address whether an additional selective pressure such as lost of androgen will be needed to progress the phenotype.

In summary, I have shown that Ack1 activity is sufficient to cause hyperplasia or mPIN when overexpressed in the murine prostate epithelium *in vivo*. Furthermore, Ack1 activity is able accelerate the onset of the prostatic phenotype when present in combination with other lesions, thus reflecting the pathophysiology of human prostate cancer.

References

1. Mahajan, N.P., et al., *Activated Cdc42-associated kinase Ack1 promotes prostate cancer progression via androgen receptor tyrosine phosphorylation.* Proc Natl Acad Sci U S A, 2007. 104(20): p. 8438-43.
2. Wang, S., et al., *Prostate-specific deletion of the murine Pten tumor suppressor gene leads to metastatic prostate cancer.* Cancer Cell, 2003. 4(3): p. 209-21.
3. Mahajan, N.P., et al., *Activated tyrosine kinase Ack1 promotes prostate tumorigenesis: role of Ack1 in polyubiquitination of tumor suppressor Wwox.* Cancer Res, 2005. 65(22): p. 10514-23.
4. Hill, R., et al., *Heterogeneous tumor evolution initiated by loss of pRb function in a preclinical prostate cancer model.* Cancer Res, 2005. 65(22): p. 10243-54.
5. Podsypanina, K., et al., *Mutation of Pten/Mmac1 in mice causes neoplasia in multiple organ systems.* Proc Natl Acad Sci U S A, 1999. 96(4): p. 1563-8.
6. Abate-Shen, C. and M.M. Shen, *Molecular genetics of prostate cancer.* Genes Dev, 2000. 14(19): p. 2410-34.
7. Nur, E.K.A., et al., *Requirement of activated Cdc42-associated kinase for survival of v-Ras-transformed mammalian cells.* Mol Cancer Res, 2005. 3(5): p. 297-305.

Appendix

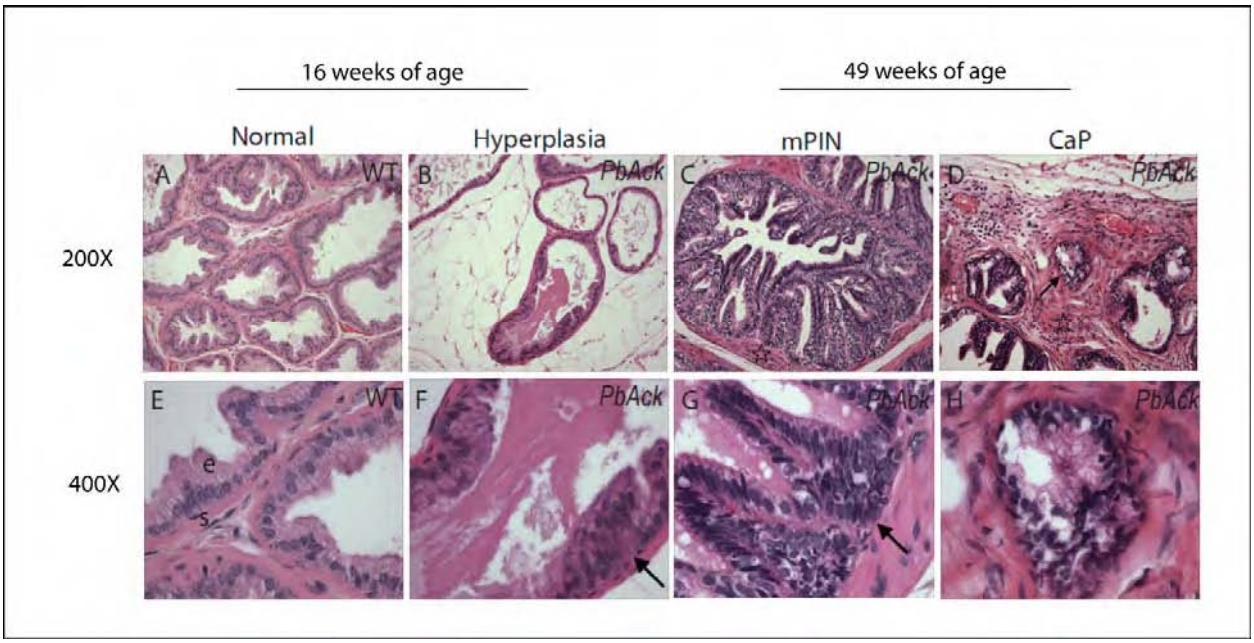

Figure 1. Histopathology of *PbAck1* prostates. Normal -vs- hyperplastic epithelia in WT (A,E) and *PbAck1* (B,F) prostates. mPIN (C,G) and microinvasive adenocarcinoma (D,H) phenotype in *PbAck1* prostate at 49 weeks of age. Hematoxylin and Eosin staining. 200X and 400X magnifications.

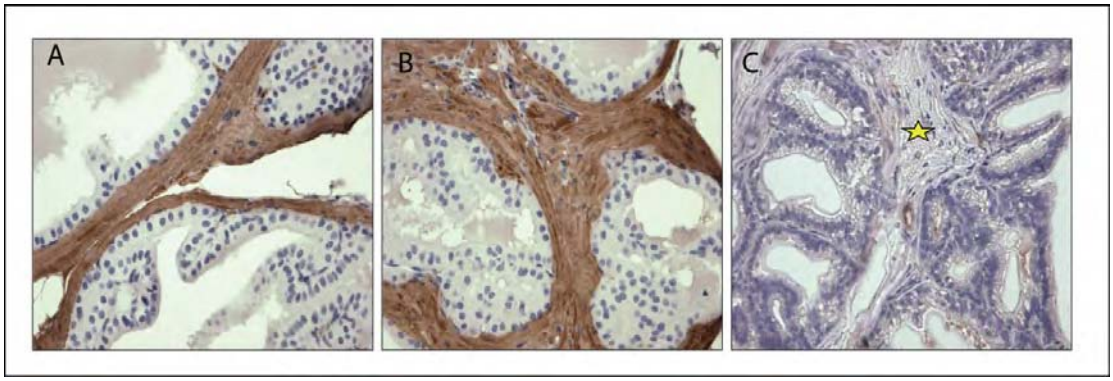

Figure 2 Desmoplastic phenotype in *PbAck1* prostate. Intact fibromuscular layer in normal WT (A) and hyperplastic *PbAck1* (B) prostates at 24 weeks of age. (C) Disruption of the fibromuscular layer (star) is evident in 49 weeks old PbAck1 prostate displaying a microinvasive adenocarcinoma phenotype. Smooth muscle actin immunohistochemistry. 400X magnification.

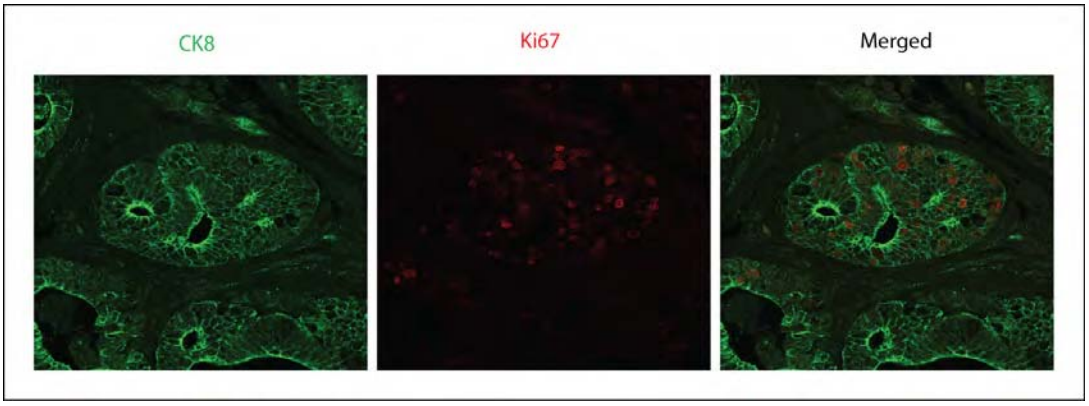

Figure 3 Hyperproliferation of luminal epithelium in PbAck1 prostates. 49 weeks old prostate from *PbAck1* immunostained for the luminal marker cytokeratin 8 (green) and the proliferation marker Ki67 (red). Double immunofluorescence. 400X magnification.

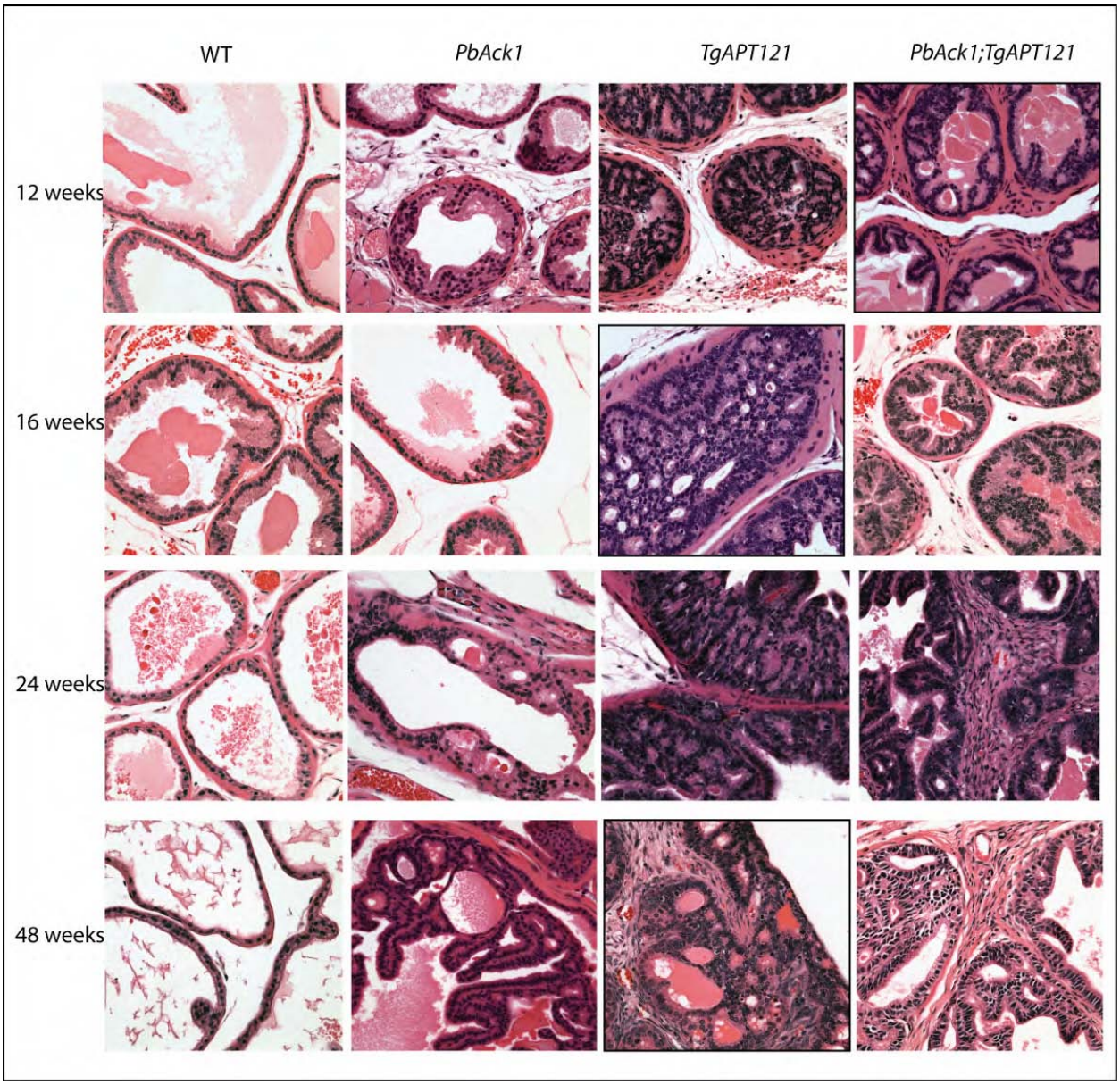

Figure 4 Histopathology of single and bi-transgenic prostates. Normal WT prostate phenotype compared to the progression from hyperplasia to mPIN to CaP in *PbAck1*, *TgAP-T_{121}* and *PbAck1;TgAP-T_{121}* prostates at 12, 16, 24 and 48 weeks of age. Hematoxylin and Eosin. 400X magnification.

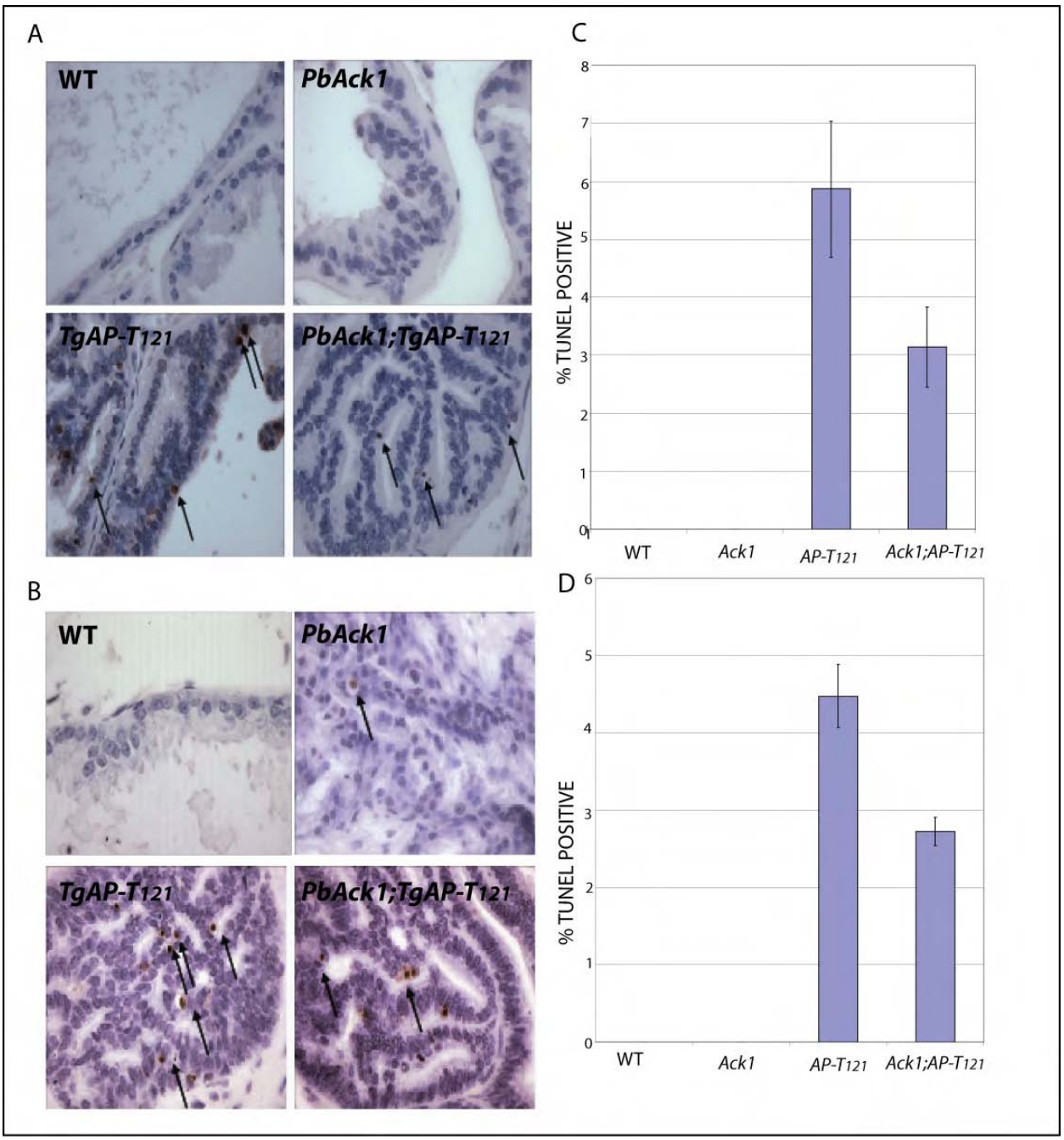

Figure 5 Decreased apoptosis in *PbAck1;TgAP-T_{121}* prostates. Prostates from 16 weeks old (A,C) and 24 weeks old (B,D) WT, *PbAck1*, *TgAP-T_{121}* and *PbAck1;TgAP-T_{121}* animals were analyzed for apoptotic levels. Apoptosis (C,D) was quantified by calculating the number of TUNEL-positive cells (brown, arrows) as a percentage of the total cells. TUNEL assay. 400X magnification. n≥3 for each genotype.

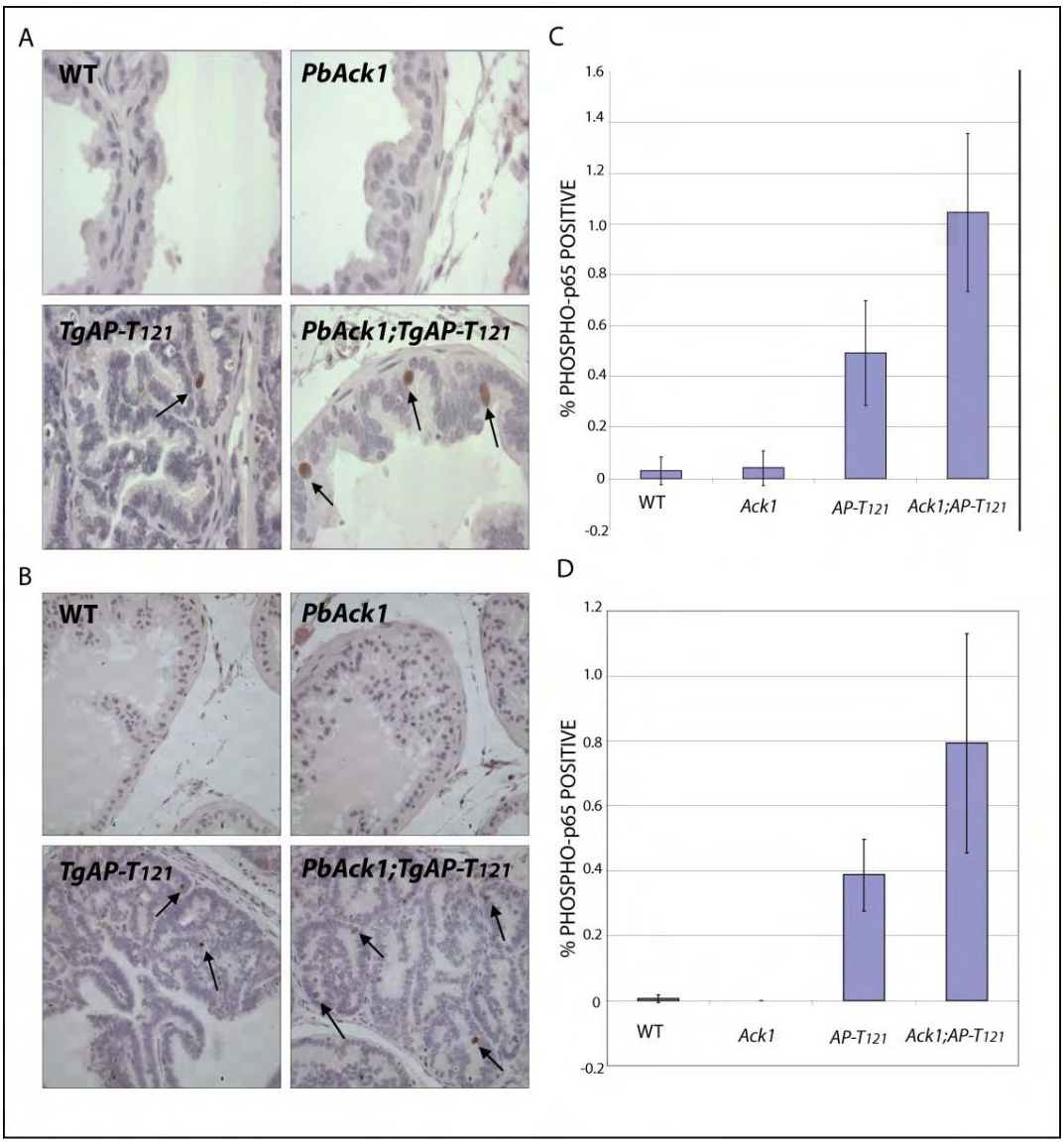

Figure 6 Increased NFκB activation in *PbAck1;TgAP-T$_{121}$* prostates. Prostates from 16 weeks old (A,C) and 24 weeks old (B,D) WT, *PbAck1*, *TgAP-T$_{121}$* and *PbAck1;TgAP-T$_{121}$* animals were analyzed for phospho-p65 levels. NFκB activation (C,D) was quantified by calculating the number of phosphor-p65-positive cells (brown, arrows) as a percentage of the total cells. Phospho-p65 immunohistochemistry. 400X magnification. n≥3 for each genotype.

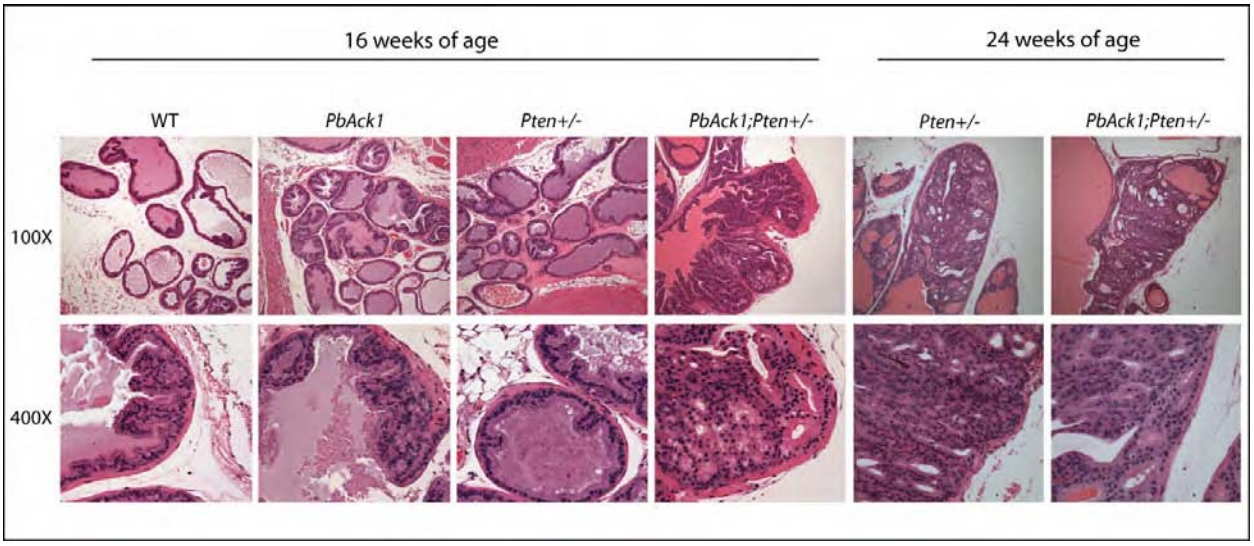

Figure 7 Histopathology of *PbAck1, Pten*$^{+/-}$ and *PbAck1;Pten*$^{+/-}$ prostates. Normal WT prostate phenotype is indistinguishable from *Pten*$^{+/-}$ at 16 weeks of age**.** *PbAck1* prostate presents hyperplasia at 16 weeks of age while *PbAck1, Pten*$^{+/-}$ prostate presents mPIN at same time point. Both *Pten*$^{+/-}$ *and PbAck1, Pten*$^{+/-}$ prostatic phenotype present mPIN at 48 weeks of age and phenotypes are indistinguishable at this point. Hematoxylin and Eosin. 100X and 400X magnification.

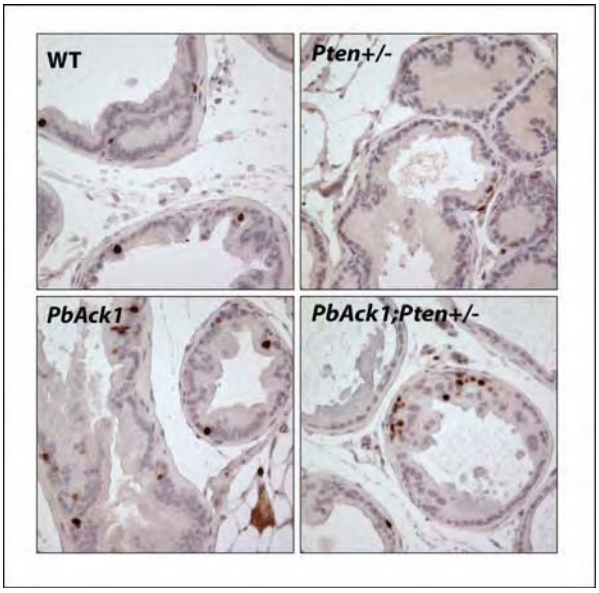

Figure 8 High localization of proliferating cells within mPIN of *PbAck1, Pten*$^{+/-}$ prostates. Proliferating cells (brown) were visualized by Ki67 immunohistochemistry. Proliferating cells were exclusively localized within the mPIN lesions in 16 week old *PbAck1, Pten*$^{+/-}$ prostates. Ki67 immunohistochemistry. 400X magnification.

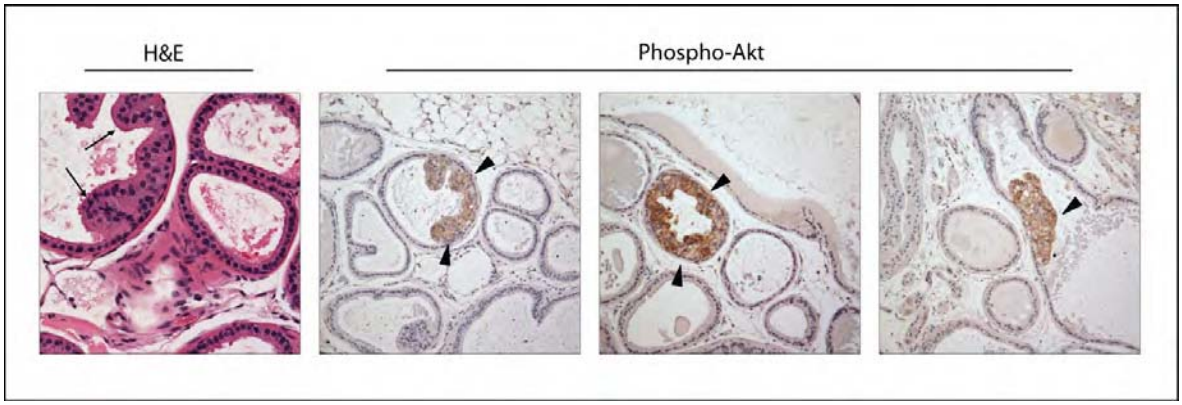

Figure 9 Akt activation within mPIN lesions of *PbAck1, Pten*$^{+/-}$ prostates. H&E shows atypical cells mPIN lesion in 16 weeks old *PbAck1, Pten*$^{+/-}$ prostate. Immunostaining for phosphor-Akt detects the presence of activated Akt (brown) within atypical cells in 16 weeks old *PbAck1, Pten*$^{+/-}$ prostates. Hematoxylin and Eosin and phosphor-Akt immunohistochemistry. 200X (H&E) and 100X (phosphor-Akt) magnifications.

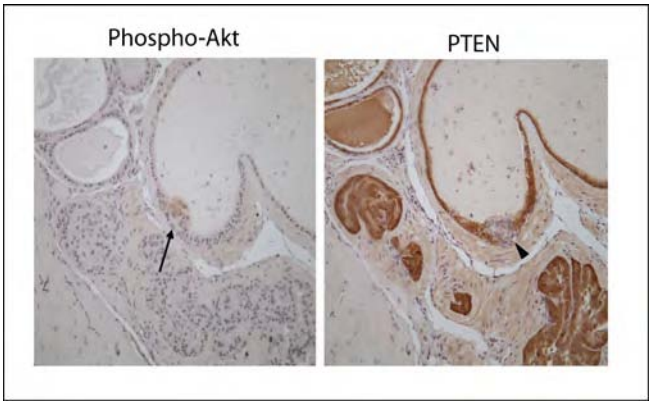

Figure 10 Correlation between loss of PTEN and activation of Akt in *PbAck1, Pten*$^{+/-}$ prostate. Sequential slides from 16 weeks old *PbAck1, Pten*$^{+/-}$ prostates were immunostained for active (phosphorylated) Akt (brown, arrow) and PTEN. PTEN is lost (arrow head) in cells positive for phospho-Akt. PTEN and phospho-Akt immunohistochemistry. 400X magnification.

OPEN ACCESS Freely available online

PLoS one

Ack1 Mediated AKT/PKB Tyrosine 176 Phosphorylation Regulates Its Activation

Kiran Mahajan[1], Domenico Coppola[2,3], Sridevi Challa[1], Bin Fang[4], Y. Ann Chen[5], Weiwei Zhu[5], Alexis S. Lopez[2], John Koomen[4], Robert W. Engelman[2], Charlene Rivera[7], Rebecca S. Muraoka-Cook[7], Jin Q. Cheng[6], Ernst Schönbrunn[1], Said M. Sebti[1], H. Shelton Earp[7], Nupam P. Mahajan[1]*

1 Drug Discovery Program, Moffitt Cancer Center, Tampa, Florida, United States of America, **2** Department of Anatomic Pathology, Moffitt Cancer Center, Tampa, Florida, United States of America, **3** Department of Experimental Therapeutics, Moffitt Cancer Center, Tampa, Florida, United States of America, **4** Proteomics Facility, Moffitt Cancer Center, Tampa, Florida, United States of America, **5** Biostatistics Division, Moffitt Cancer Center, Tampa, Florida, United States of America, **6** Department of Molecular Oncology, Moffitt Cancer Center, Tampa, Florida, United States of America, **7** Lineberger Comprehensive Cancer Center, Department of Pharmacology, University of North Carolina, Chapel Hill, North Carolina, United States of America

Abstract

The AKT/PKB kinase is a key signaling component of one of the most frequently activated pathways in cancer and is a major target of cancer drug development. Most studies have focused on its activation by Receptor Tyrosine Kinase (RTK) mediated Phosphatidylinositol-3-OH kinase (PI3K) activation or loss of Phosphatase and Tensin homolog (PTEN). We have uncovered that growth factors binding to RTKs lead to activation of a non-receptor tyrosine kinase, Ack1 (also known as ACK or TNK2), which directly phosphorylates AKT at an evolutionarily conserved tyrosine 176 in the kinase domain. Tyr176-phosphorylated AKT localizes to the plasma membrane and promotes Thr308/Ser473-phosphorylation leading to AKT activation. Mice expressing activated Ack1 specifically in the prostate exhibit AKT Tyr176-phosphorylation and develop murine prostatic intraepithelial neoplasia (mPINs). Further, expression levels of Tyr176-phosphorylated-AKT and Tyr284-phosphorylated-Ack1 were positively correlated with the severity of disease progression, and inversely correlated with the survival of breast cancer patients. Thus, RTK/Ack1/AKT pathway provides a novel target for drug discovery.

Citation: Mahajan K, Coppola D, Challa S, Fang B, Chen YA, et al. (2010) Ack1 Mediated AKT/PKB Tyrosine 176 Phosphorylation Regulates Its Activation. PLoS ONE 5(3): e9646. doi:10.1371/journal.pone.0009646

Editor: Chris Jones, Institute of Cancer Research, United Kingdom

Received October 23, 2009; **Accepted** February 10, 2010; **Published** March 19, 2010

Funding: The research was funded by Moffitt Support Grant (to N.P.M.). This work was partially supported by grants from National Institutes of Health (NIH) (R01CA120304 to H.S.E.) and the Department of Defense (W81XWH-09-1-0187 to C.R.). The funders had no role in study design, data collection and analysis, decision to publish, or preparation of the manuscript.

Competing Interests: The authors have declared that no competing interests exist.

* E-mail: nupam.mahajan@moffitt.org

Introduction

Protein kinase AKT plays a central role in growth, proliferation and cell survival [1,2,3]. AKT activation occurs when ligand binding to RTK facilitates translocation of AKT to the plasma membrane [4,5,6,7] where it is phosphorylated at Thr308 by phosphoinositide-dependent protein kinase-1 (PDK1) and at Ser473 by the 'PDK2', a class of about 10 different kinases [8] including the mTORC2 complex [9]. Phosphorylation of AKT at Thr308 and Ser473 leads to its kinase activation [10]. Upon activation, AKT phosphorylates its substrates to transduce survival signals [1,3,11,12]. During AKT activation, the first step is the production of phosphatidylinositol 3,4,5 trisphosphate (PIP3) by PI3K. PDK1 and AKT bind the phospholipid PIP3 via their PH domains and are recruited to the plasma membrane. While RTK/PI3K mediated recruitment of AKT to the plasma membrane is a well characterized mechanism, mounting evidence indicate that AKT activation can occur in a PI3K-independent fashion [13,14,15,16,17,18]. About a third of the breast and prostate tumors and majority of the pancreatic tumors that exhibit AKT activation, retain normal PTEN and PI3K activity [15] [19,20]. Interestingly, normal PTEN expression was also seen in breast, ovarian and prostate tumors that exhibit activated AKT [15]. While RTKs are suggested to be involved [21], the molecular mechanisms regulating RTK mediated AKT activation in cancers with normal PTEN and PI3K activity is poorly understood [22]. Further, *PIK3CA* activating mutation has recently been shown to be neither necessary nor sufficient for full AKT activation in situ [23]. Thus, collectively these data suggest the existence of additional pathways that regulate AKT activation in response to growth factors.

Ack1, a nonreceptor tyrosine kinase has emerged as a critical early transducer of variety of extracellular growth factor stimuli including heregulin, insulin, EGF and PDGF signaling [24,25,26,27,28]. Ack1 is ubiquitously expressed and primarily phosphorylated at Tyr284 leading to its kinase activation [25,27]. Our earlier studies demonstrated that Ack1 regulates prostate cancer progression to androgen independence by positively regulating androgen receptor (AR) and negatively regulating the tumor suppressor, Wwox [25,26,29]. Ack1 gene is also shown to be amplified in primary lung, ovarian and prostate tumors which correlated with poor prognosis [30]. In this report, we have identified a novel mechanism of Ack1 mediated AKT activation wherein phosphorylation of Tyrosine 176 in the AKT kinase domain results in its translocation to the plasma membrane and subsequent kinase activation.

Results

Ack1 Phosphorylates AKT at Evolutionary Conserved Tyr176 Resulting in AKT Activation

We observed that EGF treatment of mouse embryonic fibroblasts (MEFs) resulted in rapid Tyr-phosphorylation of Ack1 as well as Akt1 at 5 and 10 mins respectively, suggesting that these two Tyr-phosphorylation events could be linked (**Fig. 1A**). To test this hypothesis, we examined whether Ack1 could bind and Tyr-phosphorylate AKT following RTK activation. Co-immunoprecipitation of lysates derived from Akt1, Akt2, and Akt1& 2 knockout mouse embryo fibroblasts (MEF1KO, MEF2KO, and MEF1&2KO, respectively, **Fig. S1A**) that were treated with EGF, either with or without pretreatment with LY294002, a PI3K inhibitor, revealed that endogenous Akt1 (AKT here onwards) and Ack1 formed a stable complex which was not abrogated by LY294002 (**Fig. 1B**). The bottom panel shows that upon LY294002 addition there was substantial decrease in AKT Ser473-phosphorylation, suggesting that LY294002 is functional. Akt2 interacted weakly with Ack1, while Akt3 present at low levels in the MEF1&2KO cells was not detectable in the complex.

To test whether Ack1 directly phosphorylates AKT, *in vitro* binding assay was performed and AKT Tyr-phosphorylation was assessed. Myc-tagged Ack1 and HA-tagged AKT constructs were expressed and purified using respective antibody beads followed by elution, as described in methods section (**Fig. S1B**). *In vitro* binding assay revealed that purified Ack1 interacted directly with AKT resulting in AKT Tyr176-phosphorylation (**Fig. S1B–D**). Further, we generated GST-Ack construct that harbors kinase, SH3 and CRIB domain (schematic shown in **Fig. S1E**) and expressed it in *E. coli* (**Fig. S1E**) [25,31]. Androgen-receptor (AR), another Ack1 substrate [26] was expressed as FLAG-tagged construct in HEK293 cells and purified using FLAG-beads (**Fig. S1E**, left panel). GST-tagged Ack1 or GST (as control) bound to glutathione beads were incubated with purified AKT or Y176F mutant of AKT or AR (shown in **Fig. S1B** and **E**). GST-Ack1 bound to purified AKT and AR but not the Y176F mutant of AKT suggesting that AKT and AR are direct binding partners of Ack1 (**Fig. S1F**).

Affinity purification of AKT coexpressed with Ack1 (**Fig. S2A**), followed by mass spectrometry analysis revealed that AKT was phosphorylated at Tyrosine 176 (**Fig. 1C–E**). Tyr176, located in the kinase domain, is evolutionarily conserved from unicellular eukaryotes to mammals and within all the three AKT isoforms (**Fig. 1F**). Two other phosphorylation events, Ser473 and Thr308 were also identified in the same preparation (**Fig. S2B–G**). *In-silico* analysis revealed that Tyr176 and Ser473 are located in regions with increased conformational flexibility and phosphorylation at Tyr176 is likely to induce substantial conformational change and thus affect the loop harboring Ser473 (**Fig. S3**). To determine whether AKT Tyr176-phosphorylation is an upstream event that regulates AKT activation (or Ser473 phosphorylation, hereafter), site directed mutagenesis was performed to generate AKT phospho-tyrosine (Y176F) mutant (**Fig. S4A**). The Y176F mutant interacted poorly with Ack1 in the absence of ligand, and in the presence of ligand failed to interact with Ack1 resulting in decreased AKT Tyr/Ser-phosphorylations (**Fig. 1G**, lane 6). Flow cytometric analysis of EGF treated cells revealed significant reduction in Ser473-phosphorylation in MEF1&2KO cells expressing Y176F as compared to AKT (**Fig. 1H** and **Fig. S4B**). These results imply that Ack1 mediated AKT Tyr-phosphorylation results in subsequent AKT activation.

Ack1/AKT Interacting Domains

To identify domains involved in Ack1-AKT interaction, various deletions of Ack1 and AKT were generated (**Fig. S4A**). MEF1&2KO cells were co-transfected with HA-tagged AKT deletions and activated Ack1 or caAck. Immunoprecipitation using HA antibodies followed by immunoblotting with pTyr antibodies revealed Tyr-phosphorylation of full-length AKT and AKT lacking carboxy terminus (ΔCT-AKT), however, AKT deletion construct lacking the PH domain (ΔPH-AKT) exhibited significant decrease in Tyr-phosphorylation (**Fig. S4C**, top panel). The decreased phosphorylation of AKT deletion construct lacking PH domain could be due to poor binding with activated Ack1. To assess this interaction in further detail, co-immunoprecipitation experiment was performed. It revealed that in contrast to AKT or ΔCT-AKT, ΔPH-AKT weakly binds Ack1 (**Fig. S4D**, top panel). We have demonstrated that Tyr176 residue in AKT kinase domain is necessary for Ack1/AKT interaction, thus, collectively it indicates that the Ack1 need both the PH domain and tyrosine176 in AKT kinase domain for complex formation.

To identify the region in Ack1 that recognize AKT, MEF1&2KO cells were transfected with Myc-tagged Ack1 deletions (shown in **Fig. S4A**) and HA-tagged AKT. The lysates were immunoprecipitated using Myc antibodies followed by immunoblotting with AKT antibodies. The Ack1 construct expressing SAM and kinase domains (cAck) was able to bind AKT, however, construct lacking a part of kinase domain (dAck) bound poorly to endogeneous AKT (**Fig. S4E**, top panel). GST-Ack1 that possess Kinase-SH3-CRIB domains but lacking SAM domain was able to bind AKT (**Fig. S1F**). Taken together it indicates that the kinase domain in Ack1 and tyrosine176 in the kinase domain along with AKT PH domain appear to be minimal domains required for efficient Ack1/AKT complex formation.

Somatic Autoactivating Mutation (E346K) in Ack1 Activates AKT

While growth factor binding to RTK or amplification of the Ack1 gene causes Ack1 kinase activation [25,26,30], somatic autoactivating mutations in Ack1 have not yet been identified. Recently, four point mutations in Ack1, i.e. R34L, R99Q, E346K, M409I have been identified in the COSMIC database. Using site-directed mutagenesis, we generated HA-tagged point mutants (**Fig. S5A**). We tested these mutants and observed that E346K mutant undergoes autoactivation and causes AKT Tyr/Ser/Thr-phosphorylation in serum starved cells (**Fig. S5B** and **C**). Earlier we and others have characterized a point mutant (L487F mutation) that leads to constitutive activation of Ack1, also called caAck [26,32]. Both caAck(L487F mutant) and E346K auto-activating mutant of Ack1 exhibited Tyr284-phosphorylation in the activation loop (**Fig. S5D**). We also measured the intrinsic kinase activity of the Y176F mutant and the wildtype AKT in the absence and presence of activated Ack1. The wildtype AKT displays significant increase in the kinase activity as compared to the Y176F mutant when coexpressed with either one of the Ack1 constructs, E346K and caAck (**Fig. S5E** and **F**). These results demonstrate that the somatic autoactivating mutations in Ack1 are sufficient to activate AKT. Taken together with the earlier evidence indicating direct Ack1-AKT interaction, it opens an intriguing possibility of RTK/PI3K-independent AKT activation in tumors that is mediated by (auto) activated Ack1.

Tyr176-Phosphorylated AKT Translocates to the Plasma Membrane Leading to AKT Activation

Mechanistically, targeting AKT to the plasma membrane is necessary for AKT activation [1,6,7,13]. Loss of the PH domain resulted in decrease in AKT Tyr-phosphorylation upon co-expression with activated Ack1 (**Fig. S4A, C** and **D**). Further,

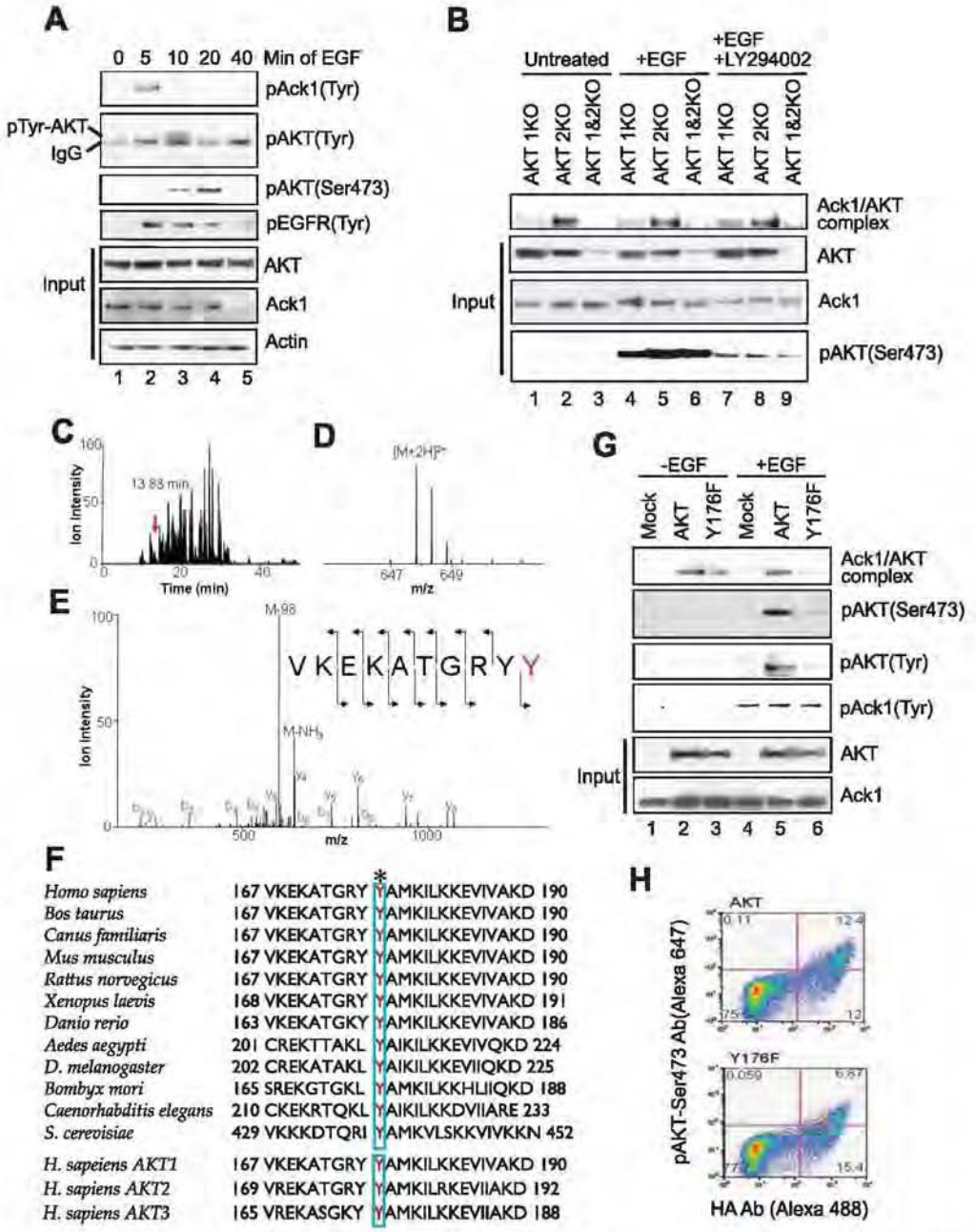

Figure 1. Tyr176 phosphorylation precedes AKT activation. (**A**) MEF2KO cells were serum starved (24 h) and treated with EGF (10 ng/ml). The lysates were immunoprecipitated or IP with anti-Ack1 (top panel), anti-AKT (second panel) and anti-EGFR (fourth panel) antibodies followed by immunoblotting or IB with anti-pTyr antibodies. Remaining panel represents IB with antibodies as shown. (**B**) MEFs were serum starved (24 h) and

treated with EGF (10 ng/ml for 10 mins) or pretreated with LY294002 (10 μM for 1 h) and EGF. The lysates were IP with Ack1 antibodies followed by IB with pan-AKT antibodies (top panel). (**C**) HA-tagged Tyr-phosphorylated AKT was purified (see Fig. S2A) followed by trypsin/chymotrypsin digestion. The peptide was detected at 13.83 mins in the total ion chromatogram (**C**) with mass-to-charge ratio 647.8132, which represents an error of 0.38 ppm (**D**). (**E**) The tandem mass spectrum matched the sequence, VKEKATGRY**pY** indicating that the C-terminal tyrosine was phosphorylated; the detection of the phosphotyrosine y_1 is consistent with this localization. (**F**) Alignment of AKT protein sequences revealed that tyrosine at 176 is invariant from yeast to humans and all the three known human AKT isoforms. (**G**) MEF1&2KO cells expressing HA-tagged AKT or Y176F mutant were serum-starved (24 h), treated with EGF for 15 mins and lysates were IP with anti-Ack1 Abs followed by IB with anti-AKT antibodies (top panel). The lysates were also IP with anti-Ack1 antibodies followed by IB with pTyr antibodies (panel 4). The same blot was stripped and IB with anti-Ack1 antibodies (Bottom panel). These lysates were also subjected to IP with anti-HA antibodies followed by IB with Ser473, pTyr and AKT antibodies (panels 2, 3 and 5, respectively). (**H**) Flow cytometry of AKT and Y176F mutant expressing MEF1&2KO cells. Cells were serum starved for 24 h, treated with EGF for 15 mins, fixed and stained with HA-antibodies conjugated to Alexa488 and phosphoSer473-antibodies conjugated to Alexa 647. Upper right quadrant represents cells which express HA-tagged AKT or Y176F mutant that are also Ser473-phosphorylated.
doi:10.1371/journal.pone.0009646.g001

Ack1 interacts with RTKs which are located in the membrane [25,26,28]. These attributes suggest that activated Ack1 could engage AKT at the plasma membrane. To investigate the role of AKT Tyr176-phosphorylation on its cellular compartmentalization, we generated phospho-antibodies that specifically recognized Tyr176-phosphorylated AKT or pTyr176-AKT (details in SI methods). The antibodies were extensively validated (**Fig. 2A**, **Fig. S6A**, also see top panels of **Fig. 2B, C and E**, **Fig. S6B**). Normal prostate epithelial cells, RWPE, exhibited pTyr176-AKT expression upon treatment with EGF and heregulin ligand (**Fig. 2A**). The pTyr176-AKT was detected when activated Ack1 was coexpressed with AKT but not the Y176F mutant. Further, incubation of the pTyr176-AKT-antibody with phosphoAKT-Y176-peptide resulted in loss of binding to Tyr176-phosphorylated AKT (**Fig. S6A**). Cell fractionation studies revealed that heregulin, insulin and EGF treatment resulted in a time-dependent accumulation of pTyr176-AKT at the plasma membrane that lead to AKT activation (**Fig. 2B, C** and **Fig. S6B**, top panels). Optimal AKT Tyr-176 phosphorylation and plasma membrane accumulation was observed at 10, 30 and 40 mins upon EGF, insulin and heregulin ligand treatments, respectively (**Fig. S6B** and **Fig. 2B, C**). To assess whether EGF mediated AKT activation is dependent upon Tyr176-phosphorylation, MEF1&2KO cells expressing AKT or Y176F mutant were treated with EGF ligand. The Y176F mutant failed to translocate to the plasma membrane and become activated by EGF (**Fig. 2D**). The basal levels of pTyr176-AKT seen in cytosolic fraction (**Fig. 2D**, panel 2, lanes 4 6) is likely to be Tyr-phosphorylated AKT3. Depletion of Ack1 by siRNA abrogated heregulin mediated AKT Tyr176-phosphorylation, plasma membrane localization and activation in MCF-7 cells (**Fig. 2E**) and MEFs (unpublished data). Further, GFP-E346K recruited dsRed-AKT but not the dsRed-Y176F mutant to the plasma membrane as assessed by immunofluorescence (**Fig. S6C–J**). Taken together, these data suggest that Ack1 is a key intermediate signaling entity necessary for RTK mediated AKT Tyr176-phosphorylation.

Ack1 Facilitates AKT Plasma Membrane Localization and Activation

Because Ack1/AKT interaction was unaffected by LY294002 treatment (**Fig. 1B**) we assessed whether AKT Tyr176-phosphorylation could occur upon inhibition of PI3K activity. First, LY294002 treatment neither affected endogenous AKT Tyr176-phosphorylation nor its membrane localization (**Fig. 3A**). Second, in contrast to Ack1 knockdown, depletion of PI3K 110α subunit by siRNA did not inhibit pTyr176-AKT levels in MCF7 cells treated with insulin (**Fig. 3B**). However, Ser473 phosphorylation of AKT was reduced upon knockdown of either Ack1 or PI3K, suggesting existence of two distinct pathways of AKT activation. Third, membrane fraction of AKT was phosphorylated at Ser473 even in the presence of LY294002 when coexpressed with activated Ack1 in serum starved MEF1&2KO cells (**Fig. S7A**, panel 2). To determine whether Tyr-phosphorylated AKT can translocate to the plasma membrane in the absence of PIP3, AKT point mutant R25C that binds PIP3 inefficiently [4] was generated (**Fig. S7B**). The R25C mutant was Tyr-phosphorylated and recruited to membrane when coexpressed with activated Ack1, in the absence of ligand (**Fig. S7C** and **D**). Interestingly, in contrast to AKT which bound PIP3, Tyr-phosphorylated AKT bound another membrane phospholipid, phosphatidic acid (PA) (**Fig. S8**). Combined together, our data indicates that RTK/Ack1 pathway could directly facilitate AKT plasma membrane localization and activation and a fraction of AKT that is Tyr176-phosphorylated can translocate to the membrane and undergo Ser473-phosphorylation even when PI3K is inhibited.

AKT Tyr176-Phosphorylation Suppresses Expression of Apoptotic Genes and Promotes Mitotic Progression

Earlier we have observed that Ack1 translocates to the nucleus upon it's Tyr-phosphorylation [26]. We assessed the localization of pTyr176-AKT when Ack1 was activated. Ligand treatment facilitated nuclear translocation of both endogenous pTyr284-Ack1 and pTyr176-AKT (**Fig. S9A**). FoxO subgroup of transcription factors are phosphorylated by AKT leading to rapid relocalization of FoxO proteins from nucleus to cytoplasm, thus, preventing transactivation of target genes [1,11,12]. FoxO proteins regulate genes involved in cell cycle arrest (*e.g. p21, p27KIP1*), cell death (*e.g. Bim-1*) and DNA repair (*e.g. GADD45*) [11]. Real time quantitative RT-PCR analysis revealed that in MEF1&2KO cells co-expressing caAck and AKT, expression of *p21, p27, Bim-1* and *GADD45* is down regulated as opposed to the activated Ack and Y176F mutant co-expressing cells (**Fig. 4A**). Consistent with this observation, depletion of Ack1 protein by siRNA resulted in increased FoxO-responsive gene expression (**Fig. 4B**).

To further understand the molecular role of Tyr176 in cell growth, we generated a HA-tagged myristoylated Y176F or myr-Y176F (**Fig. 4C**). As the myristoylated version of AKT is constitutively anchored at the membrane, it exhibits high levels of AKT activation, as seen by Thr308-phosphorylation (**Fig. S9B**). MEF1&2KO cells expressing myr-Y176F exhibited significant decrease in Thr308-phosphorylation confirming that AKT Tyr176-phosphorylation is an important event for subsequent AKT activation. Further, MEF1&2KO cells expressing myr-AKT grow exponentially as observed by an increase in the number of the double-positive HA and phospho-H3 (Ser10) stained cells, indicative of cells undergoing mitosis (**Fig. 4D**). In contrast, the number of double-positive myr-Y176F expressing cells remained unchanged after 24 hours (**Fig. 4D**). Thus, AKT Tyr176-phosphorylation can both suppress pro-apoptotic gene transcription and promote mitotic progression.

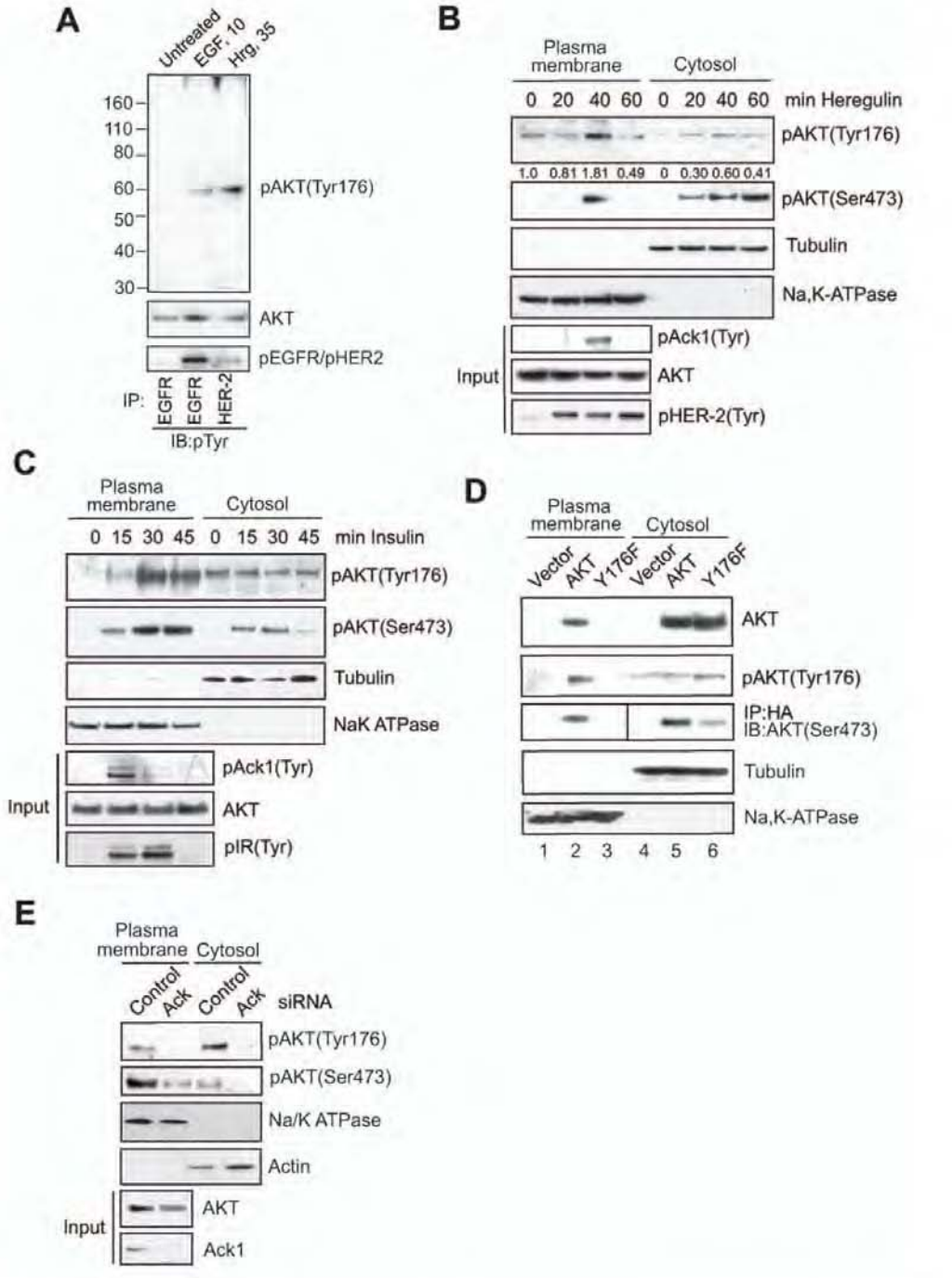
A
Untreated
EGF, 10
Hrg, 35
160
110
80
60
50
40
30
pAKT(Tyr176)
AKT
pEGFR/pHER2
IP:
EGFR
EGFR
HER-2
IB:pTyr
B
Plasma membrane
Cytosol
0 20 40 60 0 20 40 60 min Heregulin
pAKT(Tyr176)
1.0 0.81 1.81 0.49 0 0.30 0.60 0.41
pAKT(Ser473)
Tubulin
Na,K-ATPase
Input
pAck1(Tyr)
AKT
pHER-2(Tyr)
C
Plasma membrane
Cytosol
0 15 30 45 0 15 30 45 min Insulin
pAKT(Tyr176)
pAKT(Ser473)
Tubulin
NaK ATPase
Input
pAck1(Tyr)
AKT
pIR(Tyr)
D
Plasma membrane
Cytosol
Vector
AKT
Y176F
Vector
AKT
Y176F
AKT
pAKT(Tyr176)
IP:HA
IB:AKT(Ser473)
Tubulin
Na,K-ATPase
1 2 3 4 5 6
E
Plasma membrane
Cytosol
Control
Ack
Control
Ack
siRNA
pAKT(Tyr176)
pAKT(Ser473)
Na/K ATPase
Actin
Input
AKT
Ack1

Figure 2. Tyr176-phosphorylation regulates AKT plasma membrane localization. (**A**) RWPE, normal prostate epithelial cells were treated with EGF (10 ng/ml,10 mins) and heregulin (10 ng/ml, 35 mins), whole cell protein lysates were subjected to IB with indicated antibodies. (**B, C**) MCF-7 cells were serum starved (24 h) and treated with (**B**) insulin (50 ng/ml) or (**C**) heregulin (30 ng/ml) for indicated times. Cell lysates were fractionated and IB with the indicated antibodies. Input panels pAck1(Tyr), pIR(Tyr) and pHER-2(Tyr) represents IP with respective antibodies followed by IB with pTyr antibodies. (**D**) MEF 1&2KO cells were transfected with HA-tagged AKT or Y176F mutant, serum starved (24 h) and treated with EGF for 15 mins. Cell lysates were fractionated and IB with anti-HA (top panel) and indicated antibodies (bottom panels). (**E**) MCF7 cells were transfected with control or Ack1-specific siRNAs (40 nM) for 48 h and treated with heregulin for 40 mins. Cell lysates were fractionated and IB with indicated antibodies. In this experiment we have used half the volumes buffer for extraction of cytosolic proteins. Thus, the cytosolic extracts are 2X concentrated as compared to Fig. 2B–C, which explains more p176-AKT in cytosol fraction than the plasma membrane fraction.
doi:10.1371/journal.pone.0009646.g002

Probasin-Ack1 Transgenic Mice Display AKT Activation and Develop Prostatic Intraepithelial Neoplasia

We generated a transgenic mouse model in which Myc-tagged activated Ack1 was expressed under the control of modified Probasin (PB) promoter, ARR2PB (**Fig. 5A** and **B**). PB-Ack1 transgenic mice (TG) display significant increase in AKT Tyr176-phosphorylation leading to Ser473/Thr308-phosphorylation (**Fig. 5C**, top 3 panels) and AKT substrate FOXO3a Ser318/321-phosphorylation (**Fig. 5B**, panel 2) in the prostates. These mice developed intraepithelial hyperplasia by 22 weeks (**Fig. 5E**) and mPINs by 44 weeks (**Fig. 5F,J–L**). The prostate epithelium of TG mice was crowded with round to polygonal stratified nuclei, forming micropapillary projections and tufts (**Fig. 5E**). The acini were lined by a rim of basal cells (**Fig. 5F**). The areas of mPINs were easily identifiable and were characterized by prostatic acini containing intraluminal papillary structures lined by atypical cells with elongated nuclei exhibiting prominent nucleoli. Focally, the papillae merged into each other within the acini generating a cribiform pattern of growth (**Fig. 5J–L**). Dorsal lobe exhibited an increased number of small acini lined by cells containing nuclei exhibiting prominent nucleoli and the neoplastic acini were devoid of myoepithelial cells (**Fig. 5L**). We previously demonstrated that Ack1 regulates phosphorylation of androgen receptor [**26**] and tumor suppressor Wwox [25] in human prostate tumors. Neoplasia observed in PB-Ack1 mice could be due to the combined effect of Ack1 mediated AKT, AR and Wwox Tyr-phosphorylations. AR and Wwox Tyr-phosphorylations appear to be involved in late stage progression of prostate cancer to androgen-independence [26]. Ack1 mediated AKT Tyr176-phosphorylation and activation may be more proximal stage initiating processes in neoplastic progression that mimic or serve as an alternative to those of PTEN loss which has been prominently emphasized in other mouse models of prostate cancer [33].

pTyr284-Ack1 and pTyr176-AKT Expressions Correlate with Breast Cancer Progression

To examine the role of pTyr284-Ack1 and pTyr176-AKT in breast tumor progression, we performed an extensive tissue microarray analysis (TMA) of clinically annotated breast (n = 476) tumor samples. Tyr284 is the primary autophosphorylation site in Ack1, hence, phospho-Ack1(Tyr284) antibodies were used to assess Ack1 activation [27,29]. Immunohistochemical analysis revealed that pTyr284-Ack1 and pTyr176-AKT were expressed in both membrane and nucleus (**Fig. S10A,B**). A significant increase in expression of pTyr284-Ack1 and pTyr176-AKT was seen when breast cancers from progressive stages were examined, i.e. normal to hyperplasia (ADH), ductal carcinoma *in situ* (DCIS), invasive ductal carcinoma (IDC) and lymph node metastatic (LNMM) stages (**Fig. 6A–C** and **Table 1**). In contrast to pTyr284-Ack1, the total Ack1 levels remained unchanged between normal and tumor samples (compare **Fig. S10D** and **E** with **F** and **G**). ANOVA results indicated that both pTyr284-Ack1 and pTyr176-AKT expression differed significantly among progression stages ($p<0.0001$). When using Tukey-Kramer method to examine all pairwise differences between different stages, the expression levels of pTyr284-Ack1 and pTyr176-AKT

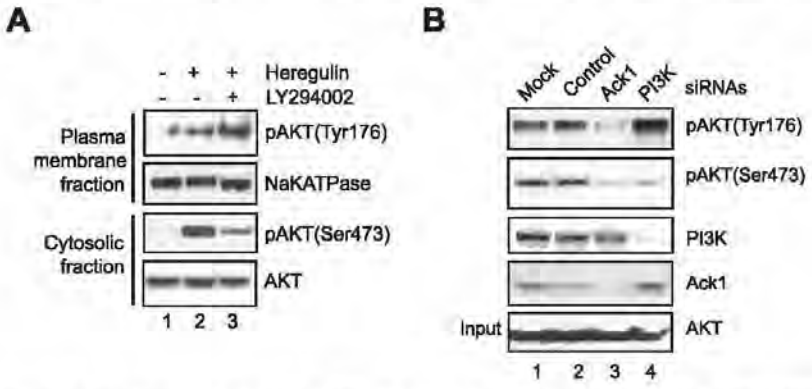

Figure 3. Tyr176-phosphorylation of AKT is PI3K-independent. (**A**) MCF-7 cells were pretreated with LY294002 (10 μM, 1 h) followed by heregulin for 40 mins. Cell lysates were fractionated and membrane fraction was subjected to IB with indicated antibodies. (**B**) MCF-7 cells were mock transfected or transfected with control, Ack1 and PI3K siRNAs, followed by insulin treatment for 30 mins. Cell lysates were subjected to IP with pTyr-antibodies, followed by IB with pTyr176-AKT antibodies (top panel). Lower panels show IB with indicated antibodies. The experiment was performed with two different Ack1 siRNAs (Qiagen).
doi:10.1371/journal.pone.0009646.g003

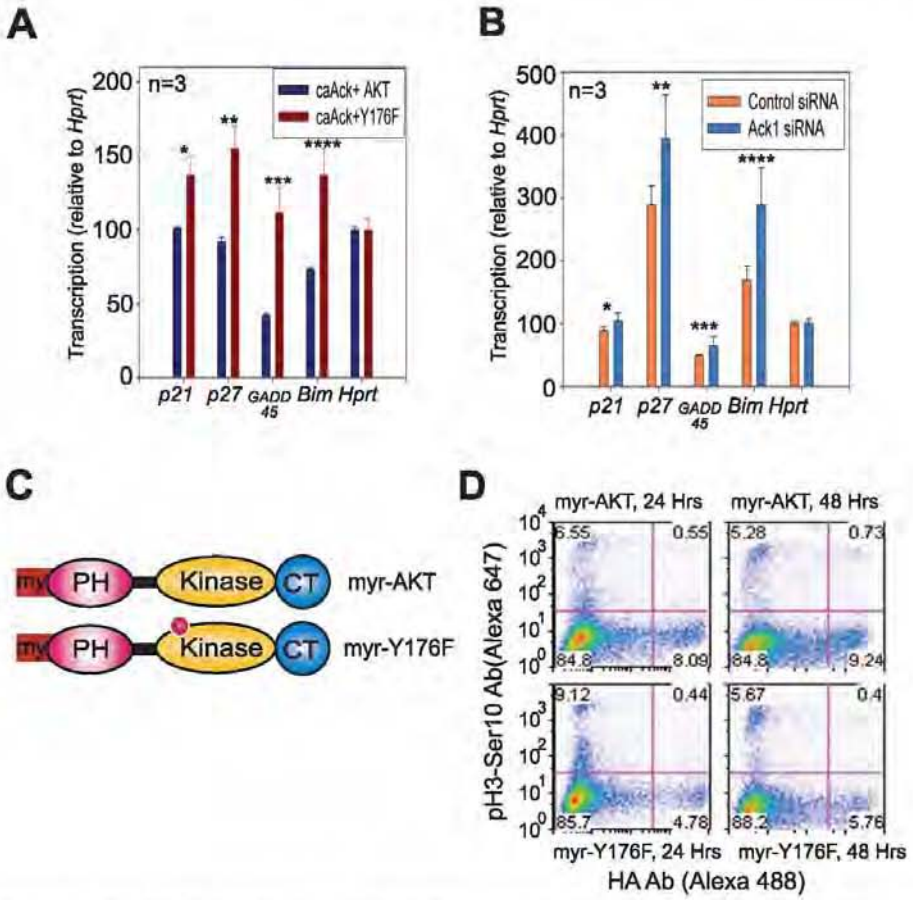

Figure 4. Tyr176 phosphorylated AKT suppresses FoxO gene transcription and promotes cell cycle progression. (**A**) MEF1&2KO cells were transfected with caAck and HA-tagged AKT or Y176F, serum starved (24 h) and harvested. Total RNA was prepared and quantitative RT-PCR was performed. Data are representative of three independent experiments. *$p \leq 0.05$; **$p \leq 0.03$; ***$p \leq 0.02$; ****$p \leq 0.02$. (**B**) MEF2KO cells were transfected with control or Ack1-specific siRNAs (40 nM) for 48 h and treated with EGF for 30 mins. Total RNA was prepared and quantitative RT-PCR was performed. *$p \leq 0.01$; **$p \leq 0.05$; ***$p \leq 0.06$; ****$p \leq 0.05$. (**C**) Schematic representation of myr-AKT and myr-Y176F point mutants. SDM of myr-AKT was performed to generate the Y176F mutation. PH, Pleckstrin homology domain; Kinase, Kinase domain and CT, Carboxy Terminal regulatory region. (**D**) AKT MEF1&2 KO cells were transfected with HA-tagged myr-AKT or myr-Y176F mutant and harvested 24 h and 48 h post-transfection. Cells were fixed and stained with anti-HA antibodies conjugated with Alexa 488 and anti-pSerine10-Histone3 conjugated with Alexa 647, a marker used to distinguish cells in late G2 and early M phase, and analyzed by flow cytometry. HA-myrAKT expressing cells showed 75% increase in the number of cells undergoing mitosis (upper right quadrant), while, HA-myrY176F-AKT expressing mitotic cells remain unchanged.

doi:10.1371/journal.pone.0009646.g004

in LNMM were significantly higher than those of all the earlier tumor stages; the expression levels were significantly lower in the normal samples when compared to those of all the later stages except for hyperplasia (**Tables 2** and **3**). Kaplan-Meir analyses revealed that patients with high expression of pTyr284-Ack1 and pTyr176-AKT are at a higher risk for cancer-related deaths (**Fig. 6D, E** and **Table 4**). Furthermore, expression of pTyr284-Ack1 was significantly correlated with pTyr176-AKT *in situ* (Spearman rank correlation coefficient $\rho = 0.43$, $p < 0.0001$; **Fig. S10C**).

Discussion

Our study indicates that cells employ multiple and possibly mutually exclusive mechanisms to activate AKT (**Fig. 7**). The reasons why RTKs would employ two distinct modes of AKT activation are not entirely clear. However, a fraction of AKT appears to utilize this alternative mode of activation in normal and prominently in cancerous cells. Our studies showed that even in the presence of PI3K inhibitor, ligand bound HER2/ErbB-2 or EGFR activated Ack1 which in turn Tyr-phosphorylated and

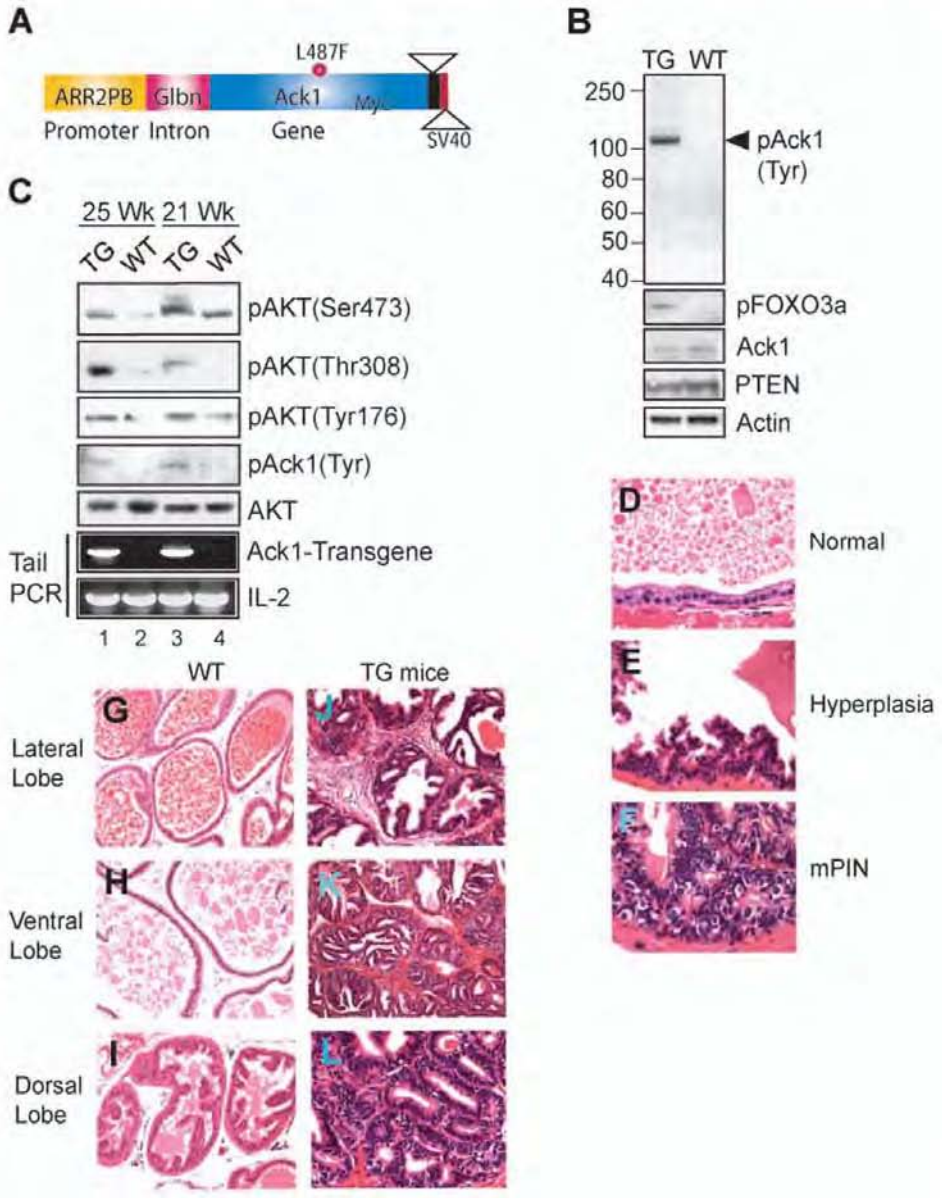

Figure 5. Probasin-Ack1 transgenic mice display pTyr176-AKT and develop mPINs. (**A**) Transgenic construct (Prob-Ack1) is shown. (**B**) A 25 wk old Probasin-Ack1 transgenic (TG) and wild type (21) male mice prostate lysates were subjected to IP using anti-Myc antibodies followed by IB with pTyr antibodies (top panel). For bottom panels, lysates were subjected to IB with indicated antibodies. (**C**) Prostate lysates from 21 and 25 wk old TG and the WT siblings were IB with respective antibodies. The bottom 2 panels represent tail-PCR of these mice. IL-2 was an internal control for PCR. (**D–L**) Haematoxylin and eosin (H&E) stained WT and TG mice prostates. Histological appearance of the prostate lateral lobe from a 22 wk old WT mouse (**D**), and corresponding lobe from age-matched TG mice with intraepithelial hyperplasia (*E*). The lateral prostate from 49 wk old TG mice exhibiting mPIN (**F**) is shown. Contrasting histological appearance of the lateral, ventral and dorsal lobes of the prostate glands from a WT mouse (**G–I**), and corresponding lobes from TG mice (49 week old) are shown (**J–L**).
doi:10.1371/journal.pone.0009646.g005

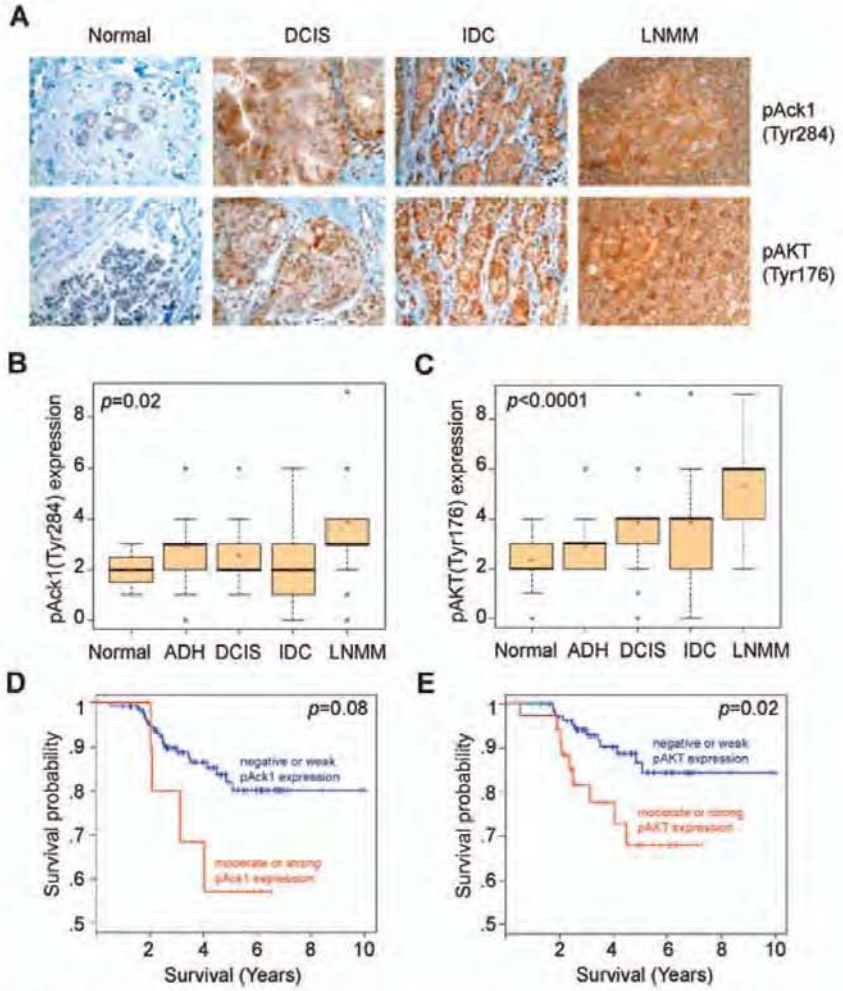

Figure 6. pTyr284-Ack1 and pTyr176-AKT expression in breast cancer. (**A**) TMA sections representing different breast cancer stages stained with pTyr284-Ack1 and pTyr176-AKT antibodies. (**B**) Box plots to summarize distributions of staining intensities for pTyr284-Ack1 in different stages of breast cancer. A significant increasing trend of intensity across progression stages was detected (Mantel-Haenszel χ^2 test, $p = 0.02$). The box has lines at the lower quartile (25%), median (50%), and upper quartile values (75%) while the red-cross within the circle marks the mean value. Whiskers extend from each end of the box to the most extreme values within 1.5 times the interquartile range from the ends of the box. The data with values beyond the ends of the whiskers, displayed with black circles, are potential outliers. (**C**) Box plots to summarize distributions of staining intensities for pTyr176-AKT in different stages of breast cancer. A significant increasing trend of intensity across progression stages was detected (Mantel-Haenszel χ^2 test, $p<0.0001$). (**D**) Kaplan–Meier analysis shows that individuals with breast cancer that have moderate to strong staining (>4) of pTyr284-Ack1 have a lower probability of survival (log rank test, $p = 0.08$). (**E**) Kaplan–Meier analysis of the breast cancer patients that have moderate to strong staining (>4) of pTyr176-AKT have significantly lower probability of survival (log rank test, $p = 0.02$).
doi:10.1371/journal.pone.0009646.g006

activated AKT. AKT is frequently activated in pancreatic cancer which has been shown to be highly correlated to HER-2/*neu* overexpression [34]. Moreover, many of the pancreatic cell lines and tumors expressing activated AKT had retained wild-type PTEN [35,36]. We noticed that PanIN, pancreatic adenocarcinoma and breast tumors of MMTV-*neu* mice exhibit significantly higher levels of pTyr284-Ack1 and pTyr176-AKT (unpublished data). Taken collectively, our data may explain AKT activation in those tumors that display amplification/activation of RTKs but have normal PI3K/PTEN levels. We propose that other tumors

Table 1. The intensities of Tyr284-phosphorylated-Ack1 and Tyr176-phosphorylated-AKT for the trend analysis of breast cancer.

Protein	Statistics	Normal	ADH	DCIS	IDC	LNMM
pTyr284-Ack1	N	52	31	38	126	39
	Mean	2	2.9	2.55	1.94	3.87
	Median	2	3	2	2	3
	Std	0.714	1.3	1.25	1.41	2
	SE	0.1	0.23	0.20	0.13	0.32
	CI Low	1.8	2.43	2.14	1.7	3.22
	CI Upper	2.2	3.38	2.96	2.19	4.52
pTyr176-AKT	N	45	39	38	118	37
	Mean	2.36	2.9	3.97	3.86	5.32
	Median	2	3	4	4	6
	Std	0.8	0.79	1.96	2.17	1.93
	SE	0.12	0.13	0.32	0.2	0.32
	CI Low	2.11	2.64	3.22	3.46	4.68
	CI Upper	2.6	3.15	4.51	4.25	5.97

doi:10.1371/journal.pone.0009646.t001

that possess somatic autoactivating mutations or amplification in non-receptor tyrosine kinases could use similar mechanisms for AKT activation [37].

Are there conditions when Tyr176 modification is not needed for AKT activation? Some of the conditions when Tyr176 phosphorylation of AKT is not required for AKT activation could be; 1) Presence of constitutively active *PIK3CA* mutations, observed in colorectal, glioblastomas, gastric breast and lung cancers [38]. 2) Loss of tumor suppressor PTEN resulting in increased levels of cellular PIP3, occur commonly in prostate cancer, endometrial cancer, and glioblastoma, among others [3]. 3) A rare somatic activating mutation, E17K in the pH domain which facilitates AKT recruitment to the membrane in PIP3-independent manner [13].

We have used the term AKT 'translocation' to indicate emergence of (cytosolic) AKT in the plasma membrane in response to growth factors. Our data (**Fig. 2B and 2C**) demonstrate that AKT in the plasma membrane is phosphorylated at Tyr 176 and mutation of this site in AKT abrogates appearance of AKT in the

Table 2. P-values of Tukey-Kramer multiple comparisons (simultaneous inference) of pTyr284-Ack1 intensity levels between all pairs of stages for breast cancer.

pTyr284-Ack1	Normal	ADH	DCIS	IDC	LMM
Normal		0.0340*	0.3324	0.9992	<0.0001*
ADH			0.8313	0.0055*	0.3324
DCIS				0.1234	0.0004*
IDC					<0.0001*
LMM					

*Indicate significance at 0.05 level.

doi:10.1371/journal.pone.0009646.t002

Table 3. P-values of Tukey-Kramer multiple comparisons (simultaneous inference) of pTyr176-AKT intensity levels between all pairs of stages for breast cancer.

pTyr176-AKT	Normal	ADH	DCIS	IDC	LMM
Normal		0.6434	0.0016*	<0.0001*	<0.0001*
ADH			0.1276	0.0342*	<0.0001*
DCIS				1.0000	0.0049*
IDC					0.0002*
LMM					

*Indicate significance at 0.05 level.

doi:10.1371/journal.pone.0009646.t003

plasma membrane (**Fig. 2D**). Based on the evidence, our model (**Fig. 7**) suggests that as Ack1 signaling pathway is initiated at the plasma membrane by RTKs. Ack1 associates with growth factor-bound RTKs (via Mig6 homology domain in Ack1 carboxy terminal proline rich region) and is activated [25,26,39]. Ack1 is constitutively bound to AKT (**Fig. 1B** and **G**). Activated Ack1 directly phosphorylates AKT at Tyr176, thus facilitating accumulation of Tyr176-phosphorylated AKT at the plasma membrane. Tyr176-phosphorylated AKT preferentially binds PA, a plasma membrane phospholipid as opposed to unphosphorylated AKT (refer to **Fig. S8** for details). PH domain in AKT is a lipid binding domain and thus might be involved in the membrane binding of Tyr176-phosphorylated AKT. Collectively, our data suggests that Ack1 mediated AKT Tyr176-phosphorylation is driving this translocation process. Thus, although AKT Tyr176-phosphorylation and its migration to the plasma membrane is PIP3 independent, the recruitment of Tyr176 AKT in the plasma membrane may require a functional PH domain.

In contrast to AKT, pTyr176-AKT specifically binds the plasma membrane anionic phospholipid, PA (**Fig. S8**). Tyr176-phosphorylation could induce conformational changes in the AKT PH domain to enable binding to PA. The PH domain of Son of sevenless (SOS) and PX domains of $p47^{phox}$ have previously been shown to possess a phosphoinositide-binding pocket and a second anion binding pocket which enables them to interact with PA facilitating plasma membrane recruitment [40,41]. We speculate that AKT too might possess a masked anion binding pocket, and Tyr-phosphorylation induced conformational changes could unmask this pocket allowing it to bind PA.

In endogenous systems Ack1 associates with AKT2 albeit weakly as compared to AKT1 (**Fig. 1B**). AKT isoforms are differentially distributed among different cellular compartments [42] with majority of AKT1 in the cytosol, and AKT2 in the mitochondria. Additionally AKT2 protein appears to be not as

Table 4. Kaplan–Meier survival estimates by Tyr284-phosphorylated Ack1 and Tyr176-phosphorylated AKT intensities for breast cancer TMA samples.

Protein	Expression	No. of subjects	Event	Censored
pTyr284-Ack1	<=4	133	14% (19)	86% (114)
pTyr284-Ack1	>4	11	36% (4)	64% (7)
pTyr176-AKT	<=4	104	11% (11)	89% (93)
pTyr176-AKT	>4	36	25% (9)	75% (27)

doi:10.1371/journal.pone.0009646.t004

Y176F) were generated by subcloning E346K and AKT cDNAs into the pEGFP-N1 and pDsRed2-N1 (Clontech) vectors respectively. Control and Ack1 siRNAs were generated by custom synthesis (Qiagen) and the sequences have been described previously [26]. PI3K siRNAs (SC39127) and antibodies were purchased from Santacruz.

AKT Phospho-Site Determination Using Mass Spectrometry

293T cells co-expressing activated Ack and HA-tagged AKT were lysed in receptor lysis buffer (RLB) containing 25 mmol/L Tris (pH 7.5), 225 mmol/L NaCl, 1% Triton X-100, 1 mmol/L DTT, 10% glycerol, phosphatase inhibitors (10 mmol/L NaF, 1 mmol/L Na_2VO_4), and protease inhibitor mix (Roche). Following immunoprecipitation with HA-beads (E6779, Sigma, St. Louis, MO), purified AKT was subjected to SDS PAGE electrophoresis and the gel was stained Coomassie Brilliant Blue-R250(BioRad). A prominent band of ~59 kDa was excised, washed once with water and twice with 50 mM ammonium bicarbonate in 50% aqueous methanol. Proteins were reduced and alkylated with 2 mM Tris(2-carboxyethyl)phosphine hydrochloride (TCEP) (Sigma, St. Louis, MO) and 20 mM iodoacetamide (GE Healthcare, Pittsburgh, PA), respectively. Samples were digested overnight with modified sequencing grade trypsin (Promega, Madison, WI), Glu-C (Worthington, Lakewood, NJ), or chymotrypsin (Roche, Switzerland). Peptides were extracted from the gel slices, phosphopeptides were enriched using IMAC spin columns (Pierce, Rockford, IL) or TiO_2 Mono tip (GL Science, Japan). A nanoflow liquid chromatograph (Ultimate3000, LC Packings/Dionex, Sunnyvale, CA) coupled to an electrospray hybrid ion trap mass spectrometer (LTQ Orbitrap, Thermo, San Jose, CA) was used for tandem mass spectrometry peptide sequencing experiments. Peptides were separated with a C18 reverse phase column (LC Packings C18Pepmap) using a 40 min gradient from 5%B to 50%B (B: 90% acetonitrile/0.1% formic acid). The flow rate on the analytical column was 300 nl/min. Five tandem mass spectra were acquired for each MS scan using 60 sec exclusion for previously sampled peptide peaks (Spray voltage 2.3 kV, 30% normalized collision energy, scanning m/z 450 1,600). Sequences were assigned using Sequest (Thermo) and Mascot (www.matrixscience.com) database searches against SwissProt protein entries of the appropriate species. Oxidized methionine, deamidation, carbamidomethyl cysteine, and phosphorylated serine, threonine and tyrosine were selected as variable modifications, and as many as 3 missed cleavages were allowed. The precursor mass tolerance was 1.08 Da and MS/MS mass tolerance was 0.8Da. Assignments were manually verified by inspection of the tandem mass spectra and coalesced into Scaffold reports (www.proteomesoftware.com).

Generation and Purification of pTyr176-AKT Phospho-Antibody

Two AKT peptides coupled to immunogenic carrier proteins were synthesized.

The phosphopeptide: Ac-ATGRY[pY]AMKIL-Ahx-C-amide

The non-phospho peptide: Ac-ATGRYYAMKIL-Ahx-C-amide

Two rabbits were immunized twice with phosphopeptide, several weeks apart, and enzyme-linked immunosorbent assay was performed to determine the relative titer of sera against phosphorylated and nonphosphorylated peptides. The titer against phosphorylated peptides (1:40,000) was much greater than nonphosphorylated peptide (1:2700). The sera were affinity-purified. In brief, two antigen-affinity columns were used to purify the phospho-specific antibodies. The first column was the non-phosphopeptide affinity column. Antibodies recognizing the non-phospho residues of the peptide bound to the column and were eluted as pan-specific antibodies. The flow-through fraction was collected and then applied to the second column, the phosphopeptide column. Antibodies recognizing the phospho-residue bound to the column which was eluted as phospho-specific antibodies. The purified antibodies were extensively characterized for various applications e.g. Western blotting and immunohistochemistry.

Cell Fractionation, Immunoprecipitations and Kinase Assay

Membrane and cytosolic fractionation was performed using kit from Biovision. The nuclear/cytoplasmic fractionation was performed using protocol from Abcam. For immunoprecipitations, cells were lysed in receptor lysis buffer (RLB) containing 25 mmol/L Tris (pH 7.5), 500 mmol/L NaCl, 1% Triton X-100, 10% glycerol, phosphatase inhibitors (10 mmol/L NaF, 1 mmol/L Na_2VO_4), and protease inhibitor mix (Roche). For co-immunoprecipitation, cells were lysed in buffer containing 25 mmol/L Tris (pH 7.5), 225 mmol/L NaCl, 1% Triton X-100, 10% glycerol, phosphatase inhibitors (10 mmol/L NaF, 1 mmol/L Na_2VO_4), and protease inhibitor mix (Roche). The kinase assay was performed using kit from Calbiochem.

Purification, *In Vitro* Binding and Phosphorylation Assay

GST-Ack1 was purified using method described earlier [31]. HEK293T cells were transfected with HA-tagged Ack1, AKT, Y176F mutant of AKT and FLAG-tagged AR; 48 hours post-transfection cell were lysed in RLB buffer. Lysates were incubated with HA beads (Sigma) for 2 h, followed by washing with RLB buffer and elution in PBS containing HA or FLAG peptide (2 mM) on ice. Purity of preparation was confirmed by coomassie blue staining of gel. For the *in vitro* binding assay, 50 nM of purified Ack and AKT were incubated in modified RLB (mRLB) containing 25 mM Tris (pH 7.5), 175 mM NaCl, 1% Triton X-100, 10% glycerol, and protease inhibitor mix at room temperature. After 30 mins, anti-Ack1 antibodies and Protein-A-sepharose beads were added, incubated with shaking at 4°C for overnight. Beads were washed thrice with mRLB buffer. Bound protein complex was dissociated from beads by boiling in SDS sample buffer and assessed by gel electrophoresis and detection by immunoblotting with anti-AKT antibody. In a control experiment, immunoprecipitation was done using non-specific IgG. For *in vitro* phosphorylation of AKT by Ack1, 50 nM of purified Ack1 and AKT were incubated in kinase buffer contained 20 mmol/L HEPES (pH 7.5), 150 mM NaCl, 10 mmol/L $MgCl_2$, 0.1 mmol/L Na_2VO_4, 0.5 mmol/L DTT, 0.25 mmol/L ATP for 1 hour at 30°C. The reaction was stopped by adding sample buffer and reaction was assessed by gel electrophoresis and detection by immunoblotting with antibodies as shown.

Quantitative RT-PCR

All RT reactions were done at the same time so that the same reactions could be used for all gene studies. For the construction of standard curves, serial dilutions of pooled sample RNA were used (50, 10, 2, 0.4, 0.08, and 0.016 ng) per reverse transcriptase reaction. One "no RNA" control and one "no Reverse Transcriptase" control were included for the standard curve. Three reactions were performed for each sample: 10 ng, 0.8 ng, and a NoRT (10 ng) control. Real-time quantitative PCR analyses were performed using the ABI PRISM 7900HT Sequence

Detection System (Applied Biosystems). All standards, the no template control (H_2O), the No RNA control, the no Reverse Transcriptase control, and the no amplification control (Bluescript plasmid) were tested in six wells per gene (2 wells/plate x 3 plates/gene). All samples were tested in triplicate wells each for the 10 ng and 0.8 ng concentrations. The no RT controls were tested in duplicate wells. PCR was carried out with SYBR Green PCR Master Mix (Applied Biosystems) using 2 µl of cDNA and the primers (**Table 5**) in a 20-µl final reaction mixture: *Actin*: 300/300 nM; *p21*: 300/300 nM; *p27Kip1*-1:300/300 nM; *p27Kip1*-2: 300/300 nM; *FASL*-2: 300/300 nM; *GADD45*-1: 300/300 nM; *GADD45*-2: 300/300 nM; *BIM*: 100/100 nM; *HPRT1*: 100/100 nM. After 2-min incubation at 50°C, AmpliTaq Gold was activated by a 10-min incubation at 95°C, followed by 40 PCR cycles consisting of 15 s of denaturation at 95°C and hybridization of primers for 1 min at 55°C. Dissociation curves were generated for each plate to verify the integrity of the primers. Data were analyzed using SDS software version 2.2.2 and exported into an Excel spreadsheet. The actin data were used for normalizing the gene values; i.e., ng gene/ng actin per well.

Fluorescence Microscopy

For cellular localization studies, NIH3T3 cells grown on coverslips were transfected at 50% confluency. Cells were fixed with 4% paraformaldehyde in PBS for 10 min, washed with PBS. Coverslips with fixed cells were mounted on slides in Vectashield mounting medium with DAPI (Vector Laboratories), and red (dsRed2-N1AKT) or green (EGFP-346K) fluorescence was detected using a Zeiss Automated Upright Fluorescent Microscope and charge-coupled device (CCD) camera with appropriate filters. Zeiss Axiovision software was used for image viewing and processing.

Ack1 Transgenic (TG) Mice

For *in vivo* expression of Ack1, Myc-epitope-tagged construct was generated in two steps. First, PCR was performed using ARR2PB promoter region (provided by UNC Mouse Core Facilities) as the template, which was subcloned in pTG1 vector. In the second step, a PCR product was generated using activated Ack1(L487F) mutant (Mahajan, 2005 #12) as the template and the reverse primer encoding a Myc-tag. The caAck PCR product (1 to 787 aa) was digested and was inserted into the pTG1 vector downstream of a sequence coding Globin intron and upstream of a SV40 polyA site (the schematic is shown in **Fig. 5A**). The construct was sequenced. The ARR2PB-Ack1 plasmid was digested with HindIII and BamHI and a 4Kb linear DNA fragment was gel purified and microinjected into fertilized C57B6 mouse eggs, which were then surgically transplanted into a pseudo-pregnant female. Transgenic founders were screened by PCR using genomic DNA isolated from tail snips. The prostate specific expression was assessed by immunoprecipitation with Myc-antibodies followed by immunoblotting with pTyr-antibodies (**Fig. 5B**). TG and WT mice were sacrificed at various time points for removal of prostate followed by lysate preparation and immunoblotting (**Fig. 5C**). Prostates from transgenic mice were dissected using a dissection microscope, fixed in 10% buffered formalin and embedded in paraffin. Sections were stained with haematoxylin and eosin and stained slides were evaluated by pathologist (R.W.E and A.S.L.).

Table 5. Primer sequences for qRT-PCR.

Primer	Sequence
p27Kip1 Fwd	TCAAACGTGAGAGTGTCTAACG
p27Kip1 Rev	CCGGGCCGAAGAGATTTCTG
p21 Fwd	TGTTCCGCACAGGAGCAA
p21 Rev	TGAGCGCATCGCAATCA
Bim Fwd	CCCGGAGATACGGATTGCAC
Bim Rev	GCCTCGCGGTAATCATTTGC
Gadd45 Fwd	AGACCGAAAGGATGGACACG
Gadd45 Rev	TGACTCCGAGCCTTGCTGA
HPRT Fwd	CACAGGACTAGAACACCTGC
HPRT Rev	GCTGGTGAAAAGGACCTCT
ACTB Fwd	GTGGGCATGGGTCAGAAG
ACTB Rev	TCCATCACGATGCCAGTG

doi:10.1371/journal.pone.0009646.t005

Flow Cytometry Analysis

AKT 1&2KO MEFs transfected with either the AKT WT or 176 mutant constructs were serum starved 24 h post-transfection. Cells were either untreated or treated with EGF for 15 minutes and harvested. Cells were singly or doubly stained with antibodies; AKT Ser473 conjugated to Alexa 647 and HA tag conjugated to Alexa 488 according to the manufacturer's protocol (Cell Signaling). Briefly, cells were resuspended in 1X Phosphate Buffered Saline (PBS) to which paraformaldehyde was added to a final concentration of 4%. Cells were fixed at 37°C for 10 min and chilled on ice for 1 min. The fixative was removed after centrifugation at 1500 rpm for 5 min. Cells were resuspended in ice cold 100% methanol and incubated on ice for 30 min and stored at -20C in 90% methanol. One million cells from each sample were rinsed with 2 ml of 1XPBS containing 0.5% BSA by centrifugation and resuspended in 90 µl of incubation buffer per assay tube for 10 min. 10 µl of conjugated antibody was added to the assay tube and incubated for 60 min in the dark at room temperature. The cells were rinsed twice with the incubation buffer by centrifugation and resuspended in 0.5 ml PBS and accquired on FACS calibur and analyzed by the FlowJo software.

Tissue Microarray (TMA) Analysis

For assessment of pTyr284-Ack1 and pTyr176-AKT expression in breast cancer, immunohistochemistry was carried out on two high-density TMAs (n = 476 cores) containing samples of normal breast tissue, atypical ductal hyperplasia (ADH), ductal carcinoma *in situ* (DCIS), invasive ductal carcinoma (IDC), lymph node macro metastasis (LNMM). Four µm sections were cut with Leica microtome (Leica Microsystems Inc, Bannockburn, IL) and transferred to adhesive-coated slides. The tissue array slides (4 slides including 2 test duplicate slides, and positive and negative controls) were stained for pTyr284-Ack1 and pTyr176-AKT using respective rabbit polyclonal antibodies. The slides were dewaxed by heating at 55 Celsius for 30 min and by three washes, 5 min each, with xylene. Tissues were rehydrated by series of 5 min washes in 100%, 95%, and 80% ethanol and distilled water. Antigen retrieval was performed by heating the samples at 95° Celsius for 30 min in 10 mmol/L sodium citrate (pH 6.0). After blocking with universal blocking serum (DAKO Diagnostic, Mississauga, Ontario, Canada) for 30 min, the samples were then incubated with rabbit polyclonal pTyr284-Ack1 antibody (1:300 dilution; Milipore) and rabbit polyclonal phospho-AKT antibody (1:25 dilution) at 4° Celsius overnight. The sections were incubated with biotin-labeled secondary and streptavidin-peroxidase for 30 min each (DAKO Diagnostic). The samples were developed with 3,3'-diaminobenzidine substrate (Vector Laboratories, Bur-

lington, Ontario, Canada) and counterstained with hematoxylin. Following standard procedures the slides were dehydrated and sealed with cover slips. Negative controls were included by omitting pTyr284-Ack1/pTyr176-AKT antibody during primary antibody incubation. The phospho-AKT/Ack1 antibodies were extensively validated for immunohistochemistry studies. MCF7 cells treated with heregulin and RWPE cells treated with EGF ligand (or no ligand) were fixed, paraffin imbedded, sectioned and used for antibody validation. Further, MEF1&2KO cells transfected with activated Ack1 and AKT were also used to validate antibodies. The pTyr284-Ack1 and pTyr176-AKT staining in paraffin embedded tissues were examined in a blinded fashion by two independent pathologists (A.L. and D.C.). If needed, a consensus score was reached for each specimen. The positive reactions were scored into four grades according to the intensity of staining: 0, 1+, 2+ and 3+. The percentages of pTyr176-AKT positive cells were also scored into four categories: 0 (0%), 1+ (1 33), 2+ (34 66), 3+ (more than 66%). The product of the intensity and percentage scores was used as a final staining score.

Statistical Analysis

The Mantel-Haenszel χ^2 test was performed to examine if there is an increasing trend for pTyr284-Ack1 and pTyr176-AKT with respect to different progression stages of breast or pancreatic cancer. The ordinal intensity levels of pTyr284-Ack1 and pTyr176-AKT 0, 1, 2, 3, 4, 6, 9 were pooled into 6 levels (as 0, 1, 2, 3, 4, and 6 and above) to accommodate the rare observations in the highest intensity level in most stages. Analysis of variance was performed to examine whether the expression levels of pTyr284-Ack1 and pTyr176-AKT differ among different tumor stages. Boxplots were used to summarize the intensity distribution at each progression stage. Furthermore, Tukey-Kramer method was performed to examine between which pairs of stages the expression levels are different. This post-hoc procedure adjusts for all pairwise comparisons and simultaneous inference. When more than one sample was obtained from a patient, the intensity of the most progressed stage was used for the analysis. Correlation between pTyr284-Ack1 and pTyr176-AKT was explored using Spearman ranked correlation analysis. The association of the expression levels of pTyr284-Ack1 and pTyr176-AKT and the overall survival of patients were assessed using the Kaplan Meier method. For breast cancer data, there were 144 individuals with available pTyr284-Ack1 staining and survival information while there were 140 individuals with available pTyr176-AKT staining and survival information. For pancreatic cancer data, there were 83 individuals with available pTyr284-Ack1 staining and survival information while there were 76 individuals with available pTyr176-AKT staining and survival information. Statistical differences between the groups were determined using log-rank test.

Supporting Information

Figure S1 AKT is Tyr-phosphorylated by Ack1 *in vitro*. (A) AKT MEF KO1, KO2 and KO1&2s lack respective AKT isoforms. Equal amounts of MEFs protein lysates were subjected to IB as indicated. MCF-7 cell lysate was used as control. (B) Purification of Ack1 and AKT. HA-tagged Ack1 and AKT were expressed in HEK293T cells, lysed and incubated with HA-beads. Followed by extensive washing, proteins were eluted using HA-peptide (2nM, 1 hour) and assessed by SDS-PAGE and Coomassie Brilliant Blue-R250(BioRad) staining. (C) *In vitro* binding assay. Equimolar amounts of purified Ack1 and AKT proteins were incubated for 30 min, complex was immunoprecipitated with Ack1 (lanes 2 5) or IgG (lane#6) antibodies followed by IB with anti-AKT antibodies (top panel). About 6.35% of total AKT was in complex with Ack1. (D) *In vitro* phosphorylation of purified AKT by Ack1. Equimolar amounts of purified Ack1 and AKT proteins were incubated in kinase buffer for 1 hour at 370C and reaction mix was subjected to IB with pTyr176-AKT (top panel), pTyr (2nd and 3rd panels), AKT (4th panel) and Ack1 (bottom panel) antibodies. (E) Schematic representation of GST-Ack1 construct. FLAG-tagged AR expressed in HEK293 cells and GST-tagged Ack1 was expressed in DH5 cells. Purified GST-Ack1 (right panel) and FLAG-AR (left panel) were assessed by SDS-PAGE followed by Coomassie staining. (F) *In vitro* binding assay. Equimolar amounts of purified HA-AKT or FLAG-AR proteins were incubated with GST-Ack1 bound to beads for overnight, beads were washed followed by IB with anti-FLAG/HA antibodies (top panel). Lower panels show IB with FLAG/HA (2nd panel) and GST (bottom panel) antibodies.
Found at: doi:10.1371/journal.pone.0009646.s001 (0.05 MB PDF)

Figure S2 Tyr176-phosphorylated AKT sample also contains Thr308 and Ser473 phosphorylated AKT. (A) Activated Ack1 (caAck) and HA-tagged AKT were coexpressed in HEK293T cells followed by IP with HA-beads. IP AKT was subjected to SDS-PAGE electrophoresis and the gel was stained Coomassie. A prominent band of ~59 kDa corresponding to AKT is seen which was excised and subjected to mass spectrometry as described in methods section. The upper ~113 kDa band corresponds to caAck1 that bound to AKT. (B) Purified AKT peptide preparation that lead to the identification of pTyr176-AKT was assessed for other phosphorylation events. A peptide was detected at 21.12 mins in the total ion chromatogram with mass-to-charge ratio 918.43, which represents an error of 1.0 ppm (C). (D) The tandem mass spectrum matched the sequence, FGLCKEGIKD-GATMKpTFC indicating that Thr308 in AKT was phosphorylated; the detection of the phosphothreonine y3 is consistent with this localization. (E) Another peptide was detected at 23.72 mins in the total ion chromatogram with mass-to-charge ratio 944.93, which represents an error of 0.99 ppm (F). (G) The tandem mass spectrum matched the sequence, ERRPHFPQFpSYSASGTA indicating that Ser473 in AKT was phosphorylated; the detection of b8, b9, y7 and y8 is consistent with this localization.
Found at: doi:10.1371/journal.pone.0009646.s002 (0.08 MB PDF)

Figure S3 AKT Tyr176-phosphorylation affects the loop harboring Ser473. (A) Residues Tyr176 and Ser473 are located in regions with increased conformational flexibility. The backbone of AKT1 is color-traced according to crystallographic B-factors from blue (20 Angstrom, less flexible) to red (76 Angstrom, highly flexible). (B) B-factor plot of all C-alpha atoms. The average main chain B-factor is 36 Angstrom (dashed horizontal line). (C) AKT Tyr176-phosphorylation induces substantial conformational changes of residues in its vicinity. Electrostatic interactions could be established with Arg174 and/or Lys214 while electrostatic repulsion and/or steric hindrance (due to the bulky phosphate group) may affect Glu169 and Tyr215. This could lead to a shift of the beta-strand flanking the c-terminal portion of the loop harboring Ser473, in turn causing structural alterations of this residue.
Found at: doi:10.1371/journal.pone.0009646.s003 (0.07 MB PDF)

Figure S4 Kinase domain of Ack1 interacts with AKT PH domain/Tyr176 in kinase domain. (A) Schematic representation of wild type AKT, Y176F point mutant and deletion constructs.

Site-directed mutagenesis of AKT was performed to generate the tyrosine to phenylalanine, Y176F, point mutant. PH, Pleckstrin homology domain; Kinase, Kinase domain and CT, Carboxy Terminal regulatory region. Schematic representation of Ack1 and deletion constructs. SAM, Sterile alpha motif; Kinase, kinase domain; SH3, Src homology domain 3; C, Cdc42 Rac interactive binding domain. (B) Flow cytometry of AKT 1&2KOMEFs, expressing HA-AKT and/or HA-Y176F. Top left panel indicates mock transfected cells stained with AKT-Ser473 antibody conjugated to Alexa 647 (untreated: 0.1%). Bottom left panel shows percentage of cells with AKT Ser473-phosphorylation upon EGF stimulation (15.2%). Right top and bottom panels show percentage of cells expressing HA-AKT (23%) or HA-Y176F (31%), respectively, in cells stained with anti-HA antibody conjugated to Alexa 488. (C) MEF1&2KO cells were co-transfected with HA-tagged AKT deletions and caAck1. The lysates were IP using HA antibodies followed by IB with pTyr antibodies (top panel). Lower panel show IP using HA antibodies followed by IB with AKT antibodies. Bottom panel show IB of the lysate with Ack1 antibodies. (D) HEK293 cells were co-transfected with HA-tagged AKT deletions and myc-tagged caAck. The lysates were IP using Myc antibodies followed by IB with HA antibodies (top panel). Lower panels are as described above. (E) MEF1&2KO cells were transfected with myc-tagged Ack1 deletions and HA-tagged AKT. The lysates were IP using Myc antibodies followed by IB with AKT antibodies (top panel). Lower panels show IB with Myc and AKT antibodies.

Found at: doi:10.1371/journal.pone.0009646.s004 (0.08 MB PDF)

Figure S5 Somatic autoactivation of Ack1. (A) Schematic representation of Ack1 and various point mutants identified in the COSMIC database. Site-directed mutagenesis of Ack1 was performed to generate four HA-tagged point mutants. SAM, Sterile alpha motif; Kinase, kinase domain; SH3, Src homology domain 3; C, Cdc42 Rac interactive binding domain; Proline, Proline rich domain; UBA, Ubiquitin binding domain. (B) E346K mutation results in Ack1 autoactivation leading to AKT activation. MEF1&2KO cells were transfected with Ack1 mutants and the lysates were IP using anti-HA antibodies followed by IB with pTyr antibodies (top panel). Lower panels show IB with indicated antibodies. (C) E346K mutant Ack1 interacts with and Tyr-phosphorylates AKT. 293T cells were co-transfected with HA-tagged Ack1 point mutants. Equal amounts of protein lysates were subjected to IP using HA antibodies. IB with AKT antibodies revealed formation of activated Ack1(E346K)/endogenous AKT complex (top panel). (D) HEK293T cells were transfected with HA-tagged E346K, caAck or kdAck (K158R) mutants. Lysates were subjected to IP using anti-HA (top panel) antibodies followed by IB with pTyr284-Ack1 antibodies. Lower panels show IB with indicated antibodies. (E) E346K or caAck mediated AKT Tyr-phosphorylation leads to AKT kinase activation. HEK293T cells were co-transfected with E346K or myc-tagged caAck and AKT or Y176F mutant. Lysates were subjected to IP using anti-myc (top panel) and anti-Ack1 (second panel) antibodies followed by IB with pTyr antibodies. The same lysates were processed for kinase assay shown in S6F. (F) Ack1 autoactivation leads to AKT kinase activation. As described in S6E, lysates were IP with HA-antibodies, followed by AKT kinase assay. Low levels of Ack1 kinase activity in vector transfected cells was treated as zero and increased kinase activity (in percentage) over the vector expressing cells is shown.

Found at: doi:10.1371/journal.pone.0009646.s005 (0.05 MB PDF)

Figure S6 Generation and validation of pTyr176-AKT phospho-antibodies. (A) EGF and heregulin treatment results in AKT Tyr176-phosphorylation. RWPE, normal prostate epithelial cells were treated with EGF (10 ng/ml,10 mins) and heregulin (10 ng/ml, 35 mins) ligand, equal amounts of protein lysates were subjected to immunoblotting as indicated. pTyr176-antibodies specifically recognizes endogenous Tyr-phosphorylated AKT following treatment with ligands. (B) Ack1 activation lead to AKT Tyr176-phosphorylation. 293T cells were co-transfected with myc-tagged caAck or kdAck and AKT or Y176F mutant. Equal amounts of protein lysates were subjected to immunoblotting with pTyr176-AKT antibodies. The pTyr176-antibodies recognize only the pTyrAKT (lane 2), but not the Y176F point mutant (lane 4). (C-J) Tyr176-phosphorylated AKT localizes at plasma membrane. NIH3T3 cells were co-transfected with EGFP-E346K mutant of Ack1 and dsRed2-N1-AKT (D-F) or dsRed2-N1-Y176F-AKT (G-J) DNAs overnight. Cells were serum starved, fixed and visualized by fluorescence microscopy. AKT but not Y176F mutant was localized to the plasma membrane in activated Ack1(E346K) expressing cells.

Found at: doi:10.1371/journal.pone.0009646.s006 (0.07 MB PDF)

Figure S7 Tyr176-phosphorylation of mutant AKT (R25C) that inefficiently binds phosphatidyl-inositol 3,4, 5-triphosphate. (A) MEF1&2KO cells were transfected with activated Ack and AKT followed by LY294002 (10 μM) for 1 h. Cell lysates were fractionated and subjected to immunoblotting with indicated antibodies. AKT Ser473 phosphorylation in membrane fraction was unaffected by LY294002 treatment suggesting Ack1 mediated AKT activation is not dependent upon PI3K activity. (B) Schematic representation of wild type AKT and R25C point mutant constructs. Site-directed mutagenesis of AKT was performed to generate the R25C point mutant. PH, Pleckstrin homology domain; Kinase, Kinase domain and CT, Carboxy Terminal regulatory region. (C) MEF1&2 KO cells were transfected with empty vector or caAck and HA-tagged AKT or R25C mutant DNAs. Serum starved (18 h) cells were treated with EGF (10 ng/ml, 15 mins). The lysates were subjected to immunoprecipitation with anti-HA (top panel) or anti-Ack1 (second panel) antibodies followed by immunoblotting with pTyr antibodies. (D) MEF1&2 KO cells were transfected with empty vector or caAck and HA-tagged AKT or R25C mutant DNAs. Serum starved (18 h) cells were treated with EGF (10 ng/ml, 15 min). Cell lysates were fractionated and subjected to immunoblotting.

Found at: doi:10.1371/journal.pone.0009646.s007 (0.05 MB PDF)

Figure S8 Tyr-phosphorylated AKT binds to phosphatidic acid. Protein-phospholipid overlay assay was performed using nitrocellulose membranes spotted with 100 pmol of different phospholipids. (A-C, F,G) Cells transfected with vector or activated Ack1 and AKT or Y176F were lysed and immunoprecipitated with pTyr-beads followed by elution with phenylphosphate. The eluted Tyr-phosphorylated proteins were incubated with phospholipid blots overnight at 4°C. Blots were extensively washed and bound proteins were detected with (A, B and F) pTyr176-AKT and (C and G) AKT antibodies. (D and E) Cells expressing HA-tagged AKT (D) and Y176F mutant (E) were lysed and immunoprecipitated with HA-beads followed by elution with HA peptide. The eluate was incubated with phospholipid blot and bound protein was detected with AKT antibodies. The pTyr176-AKT bound to phosphatidic acid, in contrast, AKT protein primarily binds to phosphatidyl-inositol 3,4,5-triphosphate (PIP3). (H) HA-peptide

and phenylphosphate eluates were immunoblotted with antibodies shown to confirm presence of desired proteins.
Found at: doi:10.1371/journal.pone.0009646.s008 (0.03 MB PDF)

Figure S9 Tyr176 phosphorylated AKT is enriched in the nucleus. (A) MCF-7 cells were serum starved (24 h) and treated with heregulin (30 ng/ml) for indicated times. Cell lysates were fractionated into nuclear and cytoplasmic fractions. Equal amounts of protein from these two fractions were subjected to immunoblotting with indicated Abs. Activated Ack1 mediated Tyr176 phosphorylated AKT is enriched in the nucleus 45 mins after heregulin treatment. The mobility of pTyr176-AKT is affected due to difference in the salt concentrations of nuclear (300 mM NaCl) and cytoplasmic fractions (10 mM KCl) (top panel). (B) MEF1&2KO cells were transfected with HA-tagged myr-AKT or myr-Y176F, equal amounts of protein lysates were subjected to immunoblotting as indicated. The myristoylated-AKT exhibits high levels of AKT activation, as seen by Thr308-phosphorylation.
Found at: doi:10.1371/journal.pone.0009646.s009 (0.03 MB PDF)

Figure S10 Staining of tumor samples with Tyr284-phosphorylated-Ack1 and Tyr176-phosphorylated-AKT antibodies. Representations of Tyr284-phosphorylated-Ack1 (A) and Tyr176-phosphorylated-AKT (B) staining of IDC, which show intense staining in nuclei and membrane. (C) Expression levels between Tyr284-phosphorylated-Ack1 and Tyr176-phosphorylated-AKT expression were significantly correlated in breast tumors (Spearman rank correlation coefficient rho = 0.43, $p<0.0001$). (D G) Breast samples stained with Ack1 and pAck1(Tyr284) antibodies. Basal levels of Ack1 expression were seen in both normal and tumor samples (D, E), however, significant increase in pAck1(-Tyr284) staining was seen in tumor samples as contrast to normal breast sample (compare F and G).
Found at: doi:10.1371/journal.pone.0009646.s010 (0.10 MB PDF)

Acknowledgments

We thank Young Whang for providing AKT cDNAs and Diana Peck Rooney for help in mice breeding. We thank Drs. Scott Powers, Donald Tindall, Todd Miller, Young Whang and Vivek Rangnekar for critical reading of the manuscript. We also thank the Molecular Biology, Flow Cytometry, Tissue Core, Proteomics Facilities at Moffitt Cancer Center and Proteomics Facilities at Lineberger Cancer Center.

Author Contributions

Conceived and designed the experiments: KM NM. Performed the experiments: KM SC BF CR RSMC NM. Analyzed the data: KM DC AC WZ AL JK RWE JQC ES SS HSE NM. Contributed reagents/materials/analysis tools: KM JQC NM. Wrote the paper: KM NM.

References

1. Manning BD, Cantley LC (2007) AKT/PKB signaling: navigating downstream. Cell 129: 1261 1274.
2. Bellacosa A, Kumar CC, Di Cristofano A, Testa JR (2005) Activation of AKT kinases in cancer: implications for therapeutic targeting. Adv Cancer Res 94: 29 86.
3. Vivanco I, Sawyers CL (2002) The phosphatidylinositol 3-Kinase AKT pathway in human cancer. Nat Rev Cancer 2: 489 501.
4. Franke TF, Yang SI, Chan TO, Datta K, Kazlauskas A, et al. (1995) The protein kinase encoded by the Akt proto-oncogene is a target of the PDGF-activated phosphatidylinositol 3-kinase. Cell 81: 727 736.
5. Burgering BM, Coffer PJ (1995) Protein kinase B (c-Akt) in phosphatidylinositol-3-OH kinase signal transduction. Nature 376: 599 602.
6. Stephens L, Anderson K, Stokoe D, Erdjument-Bromage H, Painter GF, et al. (1998) Protein kinase B kinases that mediate phosphatidylinositol 3,4,5-trisphosphate-dependent activation of protein kinase B. Science 279: 710 714.
7. Stokoe D, Stephens LR, Copeland T, Gaffney PR, Reese CB, et al. (1997) Dual role of phosphatidylinositol-3,4,5-trisphosphate in the activation of protein kinase B. Science 277: 567 570.
8. Dong LQ, Liu F (2005) PDK2: the missing piece in the receptor tyrosine kinase signaling pathway puzzle. Am J Physiol Endocrinol Metab 289: E187 196.
9. Sarbassov DD, Guertin DA, Ali SM, Sabatini DM (2005) Phosphorylation and regulation of Akt/PKB by the rictor-mTOR complex. Science 307: 1098 1101.
10. Alessi DR, Andjelkovic M, Caudwell B, Cron P, Morrice N, et al. (1996) Mechanism of activation of protein kinase B by insulin and IGF-1. Embo J 15: 6541 6551.
11. Greer EL, Brunet A (2005) FOXO transcription factors at the interface between longevity and tumor suppression. Oncogene 24: 7410 7425.
12. Huang H, Tindall DJ (2007) Dynamic FoxO transcription factors. J Cell Sci 120: 2479 2487.
13. Carpten JD, Faber AL, Horn C, Donoho GP, Briggs SL, et al. (2007) A transforming mutation in the pleckstrin homology domain of AKT1 in cancer. Nature 448: 439 444.
14. Zhao JJ, Cheng H, Jia S, Wang L, Gjoerup OV, et al. (2006) The p110alpha isoform of PI3K is essential for proper growth factor signaling and oncogenic transformation. Proc Natl Acad Sci U S A 103: 16296 16300.
15. Sun M, Wang G, Paciga JE, Feldman RI, Yuan ZQ, et al. (2001) AKT1/PKBalpha kinase is frequently elevated in human cancers and its constitutive activation is required for oncogenic transformation in NIH3T3 cells. Am J Pathol 159: 431 437.
16. Stemke-Hale K, Gonzalez-Angulo AM, Lluch A, Neve RM, Kuo WL, et al. (2008) An integrative genomic and proteomic analysis of PIK3CA, PTEN, and AKT mutations in breast cancer. Cancer Res 68: 6084 6091.
17. Hennessy BT, Smith DL, Ram PT, Lu Y, Mills GB (2005) Exploiting the PI3K/AKT pathway for cancer drug discovery. Nat Rev Drug Discov 4: 988 1004.
18. Gami MS, Iser WB, Hanselman KB, Wolkow CA (2006) Activated AKT/PKB signaling in C. elegans uncouples temporally distinct outputs of DAF-2/insulin-like signaling. BMC Dev Biol 6: 45.
19. Bose S, Chandran S, Mirocha JM, Bose N (2006) The Akt pathway in human breast cancer: a tissue-array-based analysis. Mod Pathol 19: 238 245.
20. Panigrahi AR, Pinder SE, Chan SY, Paish EC, Robertson JF, et al. (2004) The role of PTEN and its signalling pathways, including AKT, in breast cancer; an assessment of relationships with other prognostic factors and with outcome. J Pathol 204: 93 100.
21. Zhou X, Tan M, Stone Hawthorne V, Klos KS, Lan KH, et al. (2004) Activation of the Akt/mammalian target of rapamycin/4E-BP1 pathway by ErbB2 overexpression predicts tumor progression in breast cancers. Clin Cancer Res 10: 6779 6788.
22. Tibes R, Kornblau SM, Qiu Y, Mousses SM, Robbins C, et al. (2008) PI3K/AKT pathway activation in acute myeloid leukaemias is not associated with AKT1 pleckstrin homology domain mutation. Br J Haematol 140: 344 347.
23. Vasudevan KM, Barbie DA, Davies MA, Rabinovsky R, McNear CJ, et al. (2009) AKT-independent signaling downstream of oncogenic PIK3CA mutations in human cancer. Cancer Cell 16: 21 32.
24. Manser E, Leung T, Salihuddin H, Tan L, Lim L (1993) A non-receptor tyrosine kinase that inhibits the GTPase activity of p21cdc42. Nature 363: 364 367.
25. Mahajan NP, Whang YE, Mohler JL, Earp HS (2005) Activated tyrosine kinase Ack1 promotes prostate tumorigenesis: role of Ack1 in polyubiquitination of tumor suppressor Wwox. Cancer Res 65: 10514 10523.
26. Mahajan NP, Liu Y, Majumder S, Warren MR, Parker CE, et al. (2007) Activated Cdc42-associated kinase Ack1 promotes prostate cancer progression via androgen receptor tyrosine phosphorylation. Proc Natl Acad Sci U S A 104: 8438 8443.
27. Yokoyama N, Miller WT (2003) Biochemical properties of the Cdc42-associated tyrosine kinase ACK1. Substrate specificity, authphosphorylation, and interaction with Hck. J Biol Chem 278: 47713 47723.
28. Galisteo ML, Yang Y, Urena J, Schlessinger J (2006) Activation of the nonreceptor protein tyrosine kinase Ack by multiple extracellular stimuli. Proc Natl Acad Sci U S A 103: 9796 9801.
29. Mahajan K, Challa S, Coppola D, Lawrence H, Luo Y, Gevariya H, Zhu W, Chen YA, Lawrence NJ, Mahajan NP (2010) Effect of Ack1 tyrosine kinase inhibitor on ligand-independent androgen receptor activity. Prostate, manuscript in Press.
30. van der Horst EH, Degenhardt YY, Strelow A, Slavin A, Chinn L, et al. (2005) Metastatic properties and genomic amplification of the tyrosine kinase gene ACK1. Proc Natl Acad Sci U S A 102: 15901 15906.
31. Mahajan NP, Earp HS (2003) An SH2 domain-dependent, phosphotyrosine-independent interaction between Vav1 and the Mer receptor tyrosine kinase: a mechanism for localizing guanine nucleotide-exchange factor action. J Biol Chem 278: 42596 42603.
32. Kiyono M, Kato J, Kataoka T, Kaziro Y, Satoh T (2000) Stimulation of Ras guanine nucleotide exchange activity of Ras-GRF1/CDC25(Mm) upon tyrosine phosphorylation by the Cdc42-regulated kinase ACK1. J Biol Chem 275: 29788 29793.

33. Blanco-Aparicio C, Renner O, Leal JF, Carnero A (2007) PTEN, more than the AKT pathway. Carcinogenesis 28: 1379 1386.
34. Schlieman MG, Fahy BN, Ramsamooj R, Beckett L, Bold RJ (2003) Incidence, mechanism and prognostic value of activated AKT in pancreas cancer. Br J Cancer 89: 2110 2115.
35. Matsumoto J, Kaneda M, Tada M, Hamada J, Okushiba S, et al. (2002) Differential mechanisms of constitutive Akt/PKB activation and its influence on gene expression in pancreatic cancer cells. Jpn J Cancer Res 93: 1317 1326.
36. Sakurada A, Suzuki A, Sato M, Yamakawa H, Orikasa K, et al. (1997) Infrequent genetic alterations of the PTEN/MMAC1 gene in Japanese patients with primary cancers of the breast, lung, pancreas, kidney, and ovary. Jpn J Cancer Res 88: 1025 1028.
37. Yuan TL, Cantley LC (2008) PI3K pathway alterations in cancer: variations on a theme. Oncogene 27: 5497 5510.
38. Samuels Y, Wang Z, Bardelli A, Silliman N, Ptak J, et al. (2004) High frequency of mutations of the PIK3CA gene in human cancers. Science 304: 554.
39. Shen F, Lin Q, Gu Y, Childress C, Yang W (2007) Activated Cdc42-associated kinase 1 is a component of EGF receptor signaling complex and regulates EGF receptor degradation. Mol Biol Cell 18: 732 742.
40. Zhao C, Du G, Skowronek K, Frohman MA, Bar-Sagi D (2007) Phospholipase D2-generated phosphatidic acid couples EGFR stimulation to Ras activation by Sos. Nat Cell Biol 9: 706 712.
41. Karathanassis D, Stahelin RV, Bravo J, Perisic O, Pacold CM, et al. (2002) Binding of the PX domain of p47(phox) to phosphatidylinositol 3,4-bisphosphate and phosphatidic acid is masked by an intramolecular interaction. Embo J 21: 5057 5068.
42. Santi SA, Lee H (2009) The Akt isoforms are present at distinct subcellular locations. Am J Physiol Cell Physiol.
43. Chen R, Kim O, Yang J, Sato K, Eisenmann KM, et al. (2001) Regulation of Akt/PKB activation by tyrosine phosphorylation. J Biol Chem 276: 31858 31862.
44. Conus NM, Hannan KM, Cristiano BE, Hemmings BA, Pearson RB (2002) Direct identification of tyrosine 474 as a regulatory phosphorylation site for the Akt protein kinase. J Biol Chem 277: 38021 38028.
45. Cheng JQ, Lindsley CW, Cheng GZ, Yang H, Nicosia SV (2005) The Akt/PKB pathway: molecular target for cancer drug discovery. Oncogene 24: 7482 7492.